Russian Chemical Reviews **75** (7) 617 – 636 (2006) © 2006 Russian Academy of Sciences and Turpion Ltd

DOI 10.1070/RC2006v075n07ABEH003606

Phase equilibria in the W – C system and tungsten carbides

A S Kurlov, A I Gusev

Contents

I.	Introduction	617
II.	Phase equilibria and the crystal structures of phases in the W – C system	618
III.	Phase equilibria in the W – Co – C system	625
IV.	Electronic structures of tungsten carbides	626
V.	Methods of synthesis of tungsten carbides and WC – Co alloys with different grain sizes	628
VI.	Conclusion	634

Abstract. The results of experimental and theoretical investigations of phase equilibria in the W – C system and of the crystal and electronic structures of tungsten carbides are generalised. The phase diagram of the W – C system supplemented by new compounds is considered. The sequence of phase transformations associated with ordering of lower hexagonal carbide β-W_2C is analysed. The region of existence of cubic carbide γ-WC_{1-x} is discussed in detail. The generalised information on the phase equilibria in the ternary system W – Co – C, which forms the basis for the synthesis of hard alloys WC – Co, is given. Methods of synthesis of tungsten carbides and hard alloys based on them are considered. Modern methods for the synthesis of nanostructured hard alloys are discussed in detail as well as their structures and properties. The bibliography includes 131 references.

I. Introduction

Carbides of Group IV – VI transition d-metals belong to non-stoichiometric interstitial compounds.[1–4] Transition metals of Groups IVA and VA (Ti, Zr, Hf, V, Nb, Ta) form cubic carbides MC_y with the *B*1-type structure (NaCl), while the metals of Groups VA and VIA (V, Nb, Ta, Cr, Mo, W) form in addition lower hexagonal carbides M_2C_y with the *L*′3-type structure (W_2C).†

A characteristic feature of the structures of these compounds is the presence of the face-centred cubic (fcc) or hexagonal [simple or closely-packed (hcp)] metal lattice, in which the carbon atoms are located in the centre of octahedral or trigonal interstitials of the metal lattice. The metal structure changes with the formation of carbides. In carbides, the metal lattice symmetry differs from that of transition metal lattices. Group IV metals (Ti, Zr, Hf), which have the hcp structure, form carbides with the fcc metal sublattices. Metals with the body centred cubic (bcc) structure (V, Nb, Ta, Cr, Mo, W) form carbides with the cubic or hexagonal metal sublattices. The changeover of the crystal structure of metals upon formation of carbides suggests strong metal – carbon interactions and negligible interactions between carbon atoms.[5]

In carbides, the carbon atoms, that are located in the interstitial voids of the metal sublattice form a non-metal sublattice. Unoccupied interstitials are called structural vacancies and designated as □. Together with carbon atoms, they form a substitutional solution in the non-metal sublattice. The presence of structural vacancies is a characteristic feature of carbides that belong to the group of non-stoichiometric compounds. The concentration of vacancies and their distribution type have a strong effect on the properties of such carbides. The results of experimental and theoretical studies on how the distribution of atoms and vacancies affects the structure and properties of strongly non-stoichiometric compounds are generalised in monographs.[1–4,6]

Carbides of Group IV – VI transition d-metals have the highest melting points and are the hardest among all the compounds known.[3,4,7–12] Therefore, these carbides are used in manufacturing structural and tool materials capable of operating at elevated temperatures, in aggressive media and under heavy loads; they make it possible to develop protective and hard coatings, *etc*. Tungsten carbide WC is not the hardest or the most refractory compound, *viz*., its melting point (∼ 3060 K) is low as compared with non-stoichiometric carbides TiC_y, ZrC_y, HfC_y, VC_y, NbC_y and TaC_y and its hardness (18 – 22 GPa at 300 K) is also low as compared with these carbides.[3,4] However, the hardness of WC is sufficiently stable and decreases relatively slightly with the increase in temperature from 300 to 1200 – 1300 K. Moreover, as compared with carbides of other transition metals, tungsten carbide has a higher modulus of elasticity and a lower coefficient of thermal expansion. It is the combination of the aforementioned properties and their temperature stability that determines the use of WC in the production of wear-resistant hard alloys, which form the basis of all tool materials.

Tungsten carbide was first synthesised in 1893.[13] The synthesis of refractory carbides including WC from oxides, in which calcium carbide is used as the reactant, was described.[14] The industrial production of hard alloys based on WC started 20 – 25 years after its discovery and goes on at present.[15]

A S Kurlov, A I Gusev Institute of Solid State Chemistry, Urals Branch of the Russian Academy of Sciences, ul. Pervomaiskaya 91, 620219 Ekaterinburg, Russian Federation. Fax (7-3433) 74 44 95,
tel. (7-3433) 62 35 23, e-mail: kurlov@ihim.uran.ru (A S Kurlov),
tel. (7-3433) 74 73 06, e-mail: gusev@ihim.uran.ru (A I Gusev)

Received 19 September 2005
Uspekhi Khimii **75** (7) 687 – 708 (2006); translated by T Ya Safonova

† Hereinafter, the lattice types of inorganic compounds are shown according to the following book: W B Pearson *The Crystal Chemistry and Physics of Metals and Alloys* (New York, London: Wiley, 1972); in the parentheses, the typical example of a given type is shown.

The practical interest in tungsten carbide determines the active fundamental investigations of its crystal and electronic structure and also of the physicochemical properties of both WC as such and related compounds and systems that contain it. In the past 20 years, the most active studies were associated with the synthesis and application of nanocrystalline tungsten carbide.

II. Phase equilibria and the crystal structures of phases in the W – C system

In addition to tungsten and carbon, the W – C system includes two phases, namely, W_2C and WC, each having several structural modifications, which are stable in certain temperature and concentration ranges (Fig. 1).

Two successive editions of a handbook on a phase diagrams of binary alloys [16, 17] show the generalised phase diagram of the W – C system, which is mainly based on earlier diagrams of this system [18–21] and takes into account in part the results of another publication.[22] A later handbook [23] represents a phase diagram from a paper by Rudy and Hoffman,[21] while a Russian handbook [24] reproduces a phase diagram of the W – C system given in the handbook cited.[16] Relatively few authors dealt with phase equilibria in the W – C system; however, they used different designations for the discovered phases, which led to the confusion in the description of this system. Even in the handbooks,[16, 17] the table that describes the W – C system confuses the designations for the disordered hexagonal and orthorhombic W_2C phases. To avoid confusion, in this review, the designations for the W – C system are taken from Ref. 17 (corrected for the revealed mistake). As the illustration, in certain cases we also show the designations used in other sources.

Four modifications are described for lower tungsten carbide W_2C. Three of them are low-temperature β″-W_2C, intermediate β′-W_2C and high-temperature β-W_2C, which were also designated [12, 18, 21] as α-, β- and γ-W_2C, respectively. However, the structures of these modifications were proposed based on the limited experimental data. The structure of yet another modification designated as ε-W_2C (Ref. 25) was revealed sufficiently reliably in neutron diffraction studies.[25–29]

In all W_2C modifications, tungsten atoms form a hcp metal sublattice, in which one-half of octahedral interstitials are occupied by carbon atoms. These atoms are randomly distributed over the interstitials at high temperatures and are ordered at low temperatures. The possibility of the formation of several structural modifications of W_2C is associated with different types of distribution of carbon atoms. Higher carbide WC with the hexagonal structure is designated as δ-WC [α-WC (Ref. 22) or simply WC (Refs 12 and 21)]. Furthermore, the compositions between lower and higher tungsten carbides include the cubic phase γ-WC_{1-x} [designated also as β-WC (Ref. 22) or α-WC_{1-x} (Refs 12 and 21) or simply WC_{1-x}]. For the first time, tungsten carbide with the cubic structure and the unit cell parameter of 0.416 nm was synthesised [30] by its deposition from $W(CO)_6$ vapour and described as a cubic modification of W_2C. Later, a cubic carbide with a unit cell parameter of 0.425 nm was synthesised [31] in a spark discharge between the electrodes made of hexagonal WC, which were placed into a petroleum bath, and characterised also as lower carbide W_2C. Other authors [32] who also detected the cubic modification of tungsten carbide identified it as yet another high-temperature modification of W_2C. However, at present, cubic carbide γ-WC_{1-x} is considered as a structural modification of higher tungsten carbide.

Now, we discuss characteristic features of the crystal structure of phases in the W – C system.

Metallic tungsten has the bcc structure [space group $Im\bar{3}m$ (O_h^9)] of its own structural type $A2$ (type W). Such a structure is also typical of alkali metals, vanadium, niobium, tantalum, chromium and α-Fe. The crystal structure base contains two atoms in positions 2(a) with coordinates (0 0 0) and (1/2 1/2 1/2).

According to studies by Rudy *et al.*[18–21] and in line with the phase diagram of the W – C system (see Fig. 1), the most high-temperature phase β-W_2C has a hexagonal [space group $P6_3/mmc$ (D_{6h}^4)] structure of the $L'3$-type (Fig. 2). The existence of lower

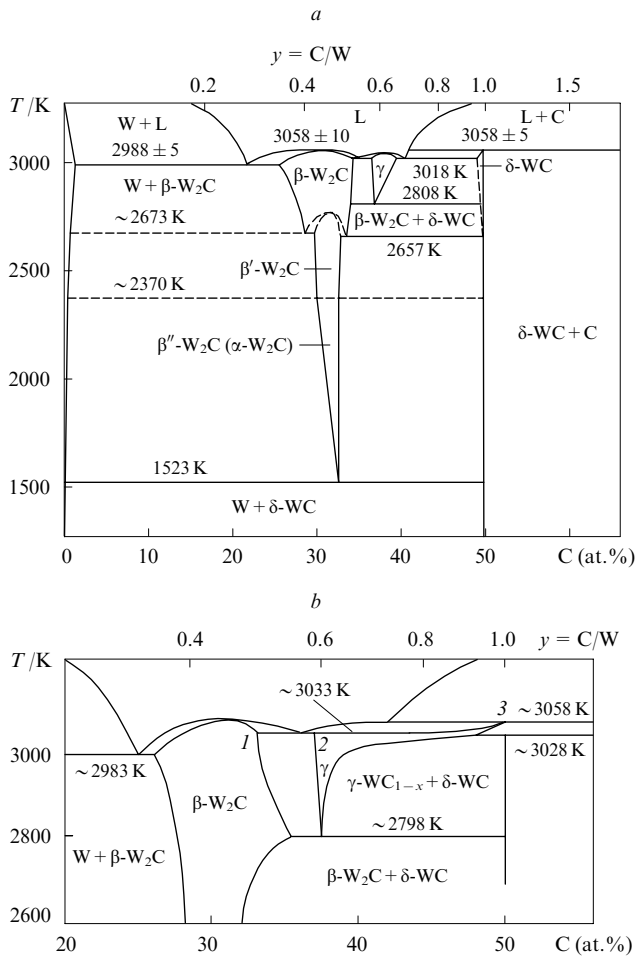


Figure 1. Generalised phase diagram of the W – C system (*a*) (see Refs 16, 17) and a fragment of this diagram in the high temperature region (*b*) (see Ref. 22).

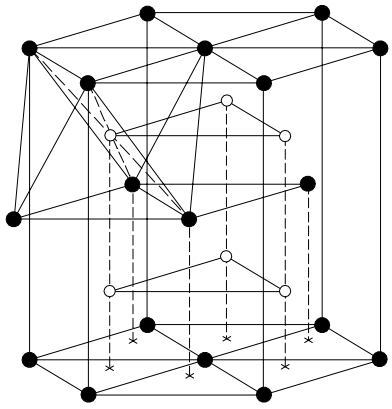


Figure 2. Hexagonal structure of the $L'3$-type of lower disordered carbide β-W_2C.[1, 2]
Tungsten atoms (solid circles) form a hcp sublattice the octahedral interstitials (open circles) of which are randomly occupied by carbon atoms with a probability of 1/2.

tungsten carbide W_2C with the $L'3$-type structure was directly proved in a neutron diffraction study,[25] in which the disordered W_2C phase was observed together with the ordered phase of this carbide. For high-temperature totally disordered W_2C, the $L'3$-type structure is quite reasonable by analogy with other lower carbides and nitrides. Particularly, the $L'3$-type hexagonal structure is typical of most non-stoichiometric lower carbides and nitrides M_2X_y (M = V, Nb, Ta; X = C, N) with the exception of V_2N. In the unit cell of β-W_2C, two tungsten atoms occupy the positions 2(*c*) with coordinates (1/3 2/3 1/4) and (2/3 1/3 3/4) and one carbon atom is randomly distributed between positions 2(*a*) with coordinates (0 0 0) and (0 0 1/2). In other words, the hexagonal β-W_2C phase is disordered, and its carbon atoms randomly occupy one-half of all octahedral interstitials in the tungsten sublattice; hence, the probability of the occupation of any octahedral interstitial is equal to 1/2. In the β-W_2C structure, along the *c* axis, the A and B layers formed by metal atoms alternate with the X layers formed by the non-metal lattice sites in the ... AXBXAXBX ... sequence . The hexagonal β-W_2C phase has a homogeneity region from $WC_{0.34}$ to $WC_{0.52}$ and is stable in the temperature range from 2670 – 2720 K to the melting temperature at 3000 – 3050 K. The unit cell parameters of the β-W_2C phase with the composition $WC_{0.52}$ were recorded[9] to be $a = 0.2992$, $c = 0.4722$ nm and are somewhat larger, *viz.*, $a = 0.3002$ and $c = 0.475 – 0.476$ nm according to data from Ref. 19.‡

In the X-ray diffraction experiments, the modifications of lower tungsten carbide, namely, β-W_2C, β′-W_2C, β″-W_2C and ε-W_2C, are virtually indistinguishable, because they have the same hexagonal metal sublattice and the scattering power of tungsten atoms is many times higher as compared with carbon atoms. Indeed, according to calculations, the changes in the carbon atom distribution in the W_2C lattice are reflected in the X-ray diffraction spectrum only in the range of small angles (Fig. 3). The intensities of $(110)_{orthorhomb}$, $(111)_{orthorhomb}$ reflections typical of orthorhombic carbide β′-W_2C, $(001)_{C6}$ reflections of carbide β″-W_2C with the *C*6-type structure and also $(101)_\varepsilon$ reflections typical of ε-W_2C do not exceed 0.5% of the intensity of the strongest reflection $(101)_{L'3}$ [or $(101)_{C6}$, $(121)_{orthorhomb}$, $(210)_\varepsilon$ of the corresponding structure]. In other words, in a real X-ray diffraction study, these reflections are well at the background level and far below the experimental error of intensity measurements.

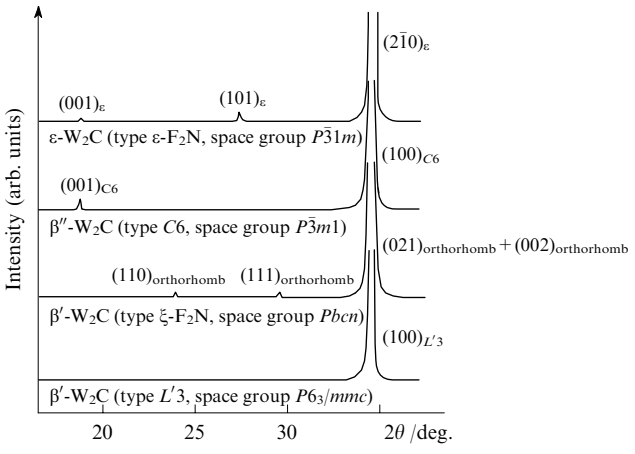


Figure 3. X-Ray diffraction patterns (Cu $K\alpha_{1,2}$ radiation) of different modifications of lower carbide W_2C in the small angle 2θ range for the $WC_{0.50}$ composition, calculated without regard for atomic displacements.[18,21]

‡ Unit cell parameters of all phases discussed in this review were obtained for quenched samples at room temperature.

The modification β′-W_2C of lower tungsten carbide has the rhombic symmetry, although its metal sublattice retains a hexagonal closely packed structure similar to the structure of high-temperature carbide β-W_2C. The structure of orthorhombic β′-W_2C is not yet known with certainty, but can be assigned to the PbO_2 type with the space group *Pbcn* (D_{2h}^{14}). For this structure, the atomic positions can be specified only in general, namely, the carbon atoms occupy positions 4(*c*) with coordinates (0 *y* 1/4) and the tungsten atoms are in positions 8(*d*) with coordinates (*x y z*). Based on the comparison of experimental and theoretical positions of the reflections in the X-ray diffraction pattern, it was concluded[18] that lower carbide β′-W_2C (β-W_2C) has an orthorhombic structure similar to the ζ-Fe_2N-type structure of ordered carbide Mo_2C and pertains to the same space group *Pbcn*.[33] However, as was noted above, the hexagonal disordered, trigonal and orthorhombic modifications of W_2C with the same unit cell parameters of the disordered phase are indistinguishable as regards the positions of their X-ray reflections at $2\theta > 30°$. In the range of small angles $2\theta < 30°$, in which the X-ray diffraction spectra are slightly different (see Fig. 3), no reflections were observed[18] and no attempts were undertaken to estimate their possible intensities. Thus, the literature contains no experimental structural data which would substantiate the detection of the orthorhombic lower tungsten carbide β′-W_2C. Moreover, the authors of the study[18] incorrectly determined the coordinates of tungsten atoms in the suggested structure of β′-W_2C carbide [the positions 8(*d*) occupied by tungsten atoms were claimed to have the coordinates (3/8 ~3/8 ~1/2)].

The unit cell of orthorhombic carbide β′-W_2C has the parameters $a = 0.4728$, $b = 0.6009$ and $c = 0.5193$ nm.[18] Our analysis of the distribution of atoms in this unit cell, which is a derivative of the hexagonal cell with the $L'3$-type structure has shown that tungsten atoms occupy 8(*d*) positions with coordinates (1/4 ~1/8 ~1/12) and carbon atoms are in 4(*c*) positions with coordinates (0 ~3/8 1/4). As compared with the high-temperature hexagonal phase β-W_2C (Fig. 4 *a*), the β′-W_2C phase with

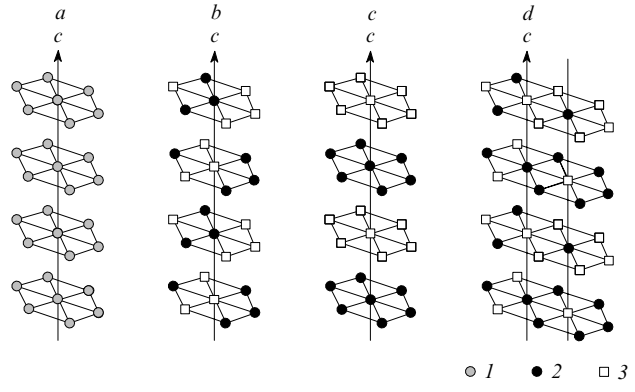


Figure 4. Distribution of carbon atoms in lower carbides β-W_2C (*a*), β′-W_2C (*b*), β″-W_2C (*c*) and ε-W_2C (*d*), which are ideal as regards both their compositions and structures.
Planes formed by the non-metal sublattice sites are located normally to the *c* axis of the basic disordered structure of the $L'3$-type; tungsten atoms are not shown.[2]
(*a*) the $L'3$-type of β-W_2C carbide with the random distribution of carbon atoms and vacancies; (*b*) β′-W_2C carbide of the Mo_2C (ζ-Fe_2N) type with the ordered distribution of carbon atoms and vacancies in each plane of the non-metal sublattice; (*c*) β″-W_2C (α-W_2C) carbide of the *C*6 type with the ordered distribution of carbon atoms and vacancies in the alternating vacant and carbon-atom-occupied planes of the non-metal sublattice; (*d*) ε-W_2C carbide of the ε-Fe_2N type with alternating planes of the non-metal sublattice, in which each vacancy is surrounded by six carbon atoms or each carbon atom is surrounded by six vacancies; (*1*) positions of non-metal interstitial atoms, which are randomly occupied by carbon atoms with a probability of 1/2; (*2*) carbon atoms; (*3*) vacancies.

the ζ-Fe_2N-type structure (Fig. 4 *b*) is ordered with respect to the non-metal sublattice. It is assumed that orthorhombic carbide β′-W_2C has the homogeneity region from $WC_{0.34}$ to $WC_{0.49}$ and exists in an intermediate temperature interval from ~2370 K to 2670–2750 K (see Fig. 1). The later studies failed to detect the orthorhombic (space group *Pbcn*) phase of β′-W_2C.

The low-temperature phase β″-W_2C (α-W_2C) is ordered, but the temperature range of its existence and its crystal structure are not yet reliably determined. An electron-diffraction study [34] dealt with lower tungsten carbide, which was synthesised by carburisation of a thin metal tungsten film in the carbon monoxide atmosphere at ~1400 K for 5 min. The diffraction pattern of this carbide revealed 74 reflections, which pointed to the ordering of carbon atoms. Presumably, the β″-W_2C phase has the *C*6 (*anti*-CdI_2)-type structure with the space group No. 164 – $P\bar{3}m1$ (D^3_{3d}); other possible ways of ordering were ignored. In the rhombohedral (trigonal) structure of the *C*6 type, the layers of carbon atoms regularly alternate with the layers of structural vacancies, being oriented normally to the *c* axis. The layers formed solely by carbon atoms are located between the pairs of layers AB formed by tungsten atoms, and the layers of vacant interstitials, *i.e.*, structural vacancies, are located between the pairs of metal layers BA (Fig. 4 *c*). Note that according to data,[34] tungsten atoms occupy virtually ideal positions in the lattice ($z = 0.25$), although the spaces along the *c* axis between the metal layers separated by the layers of vacancies should be slightly shorter than the spaces between the metal layers separated by a carbon-atom layer.

Thus, the ideal structure of β″-W_2C (α-W_2C) contains two tungsten atoms in positions 2(*d*) with coordinates (1/3 2/3 1/4) and (2/3 1/3 3/4), a carbon atom in position 1(*a*) with coordinates (0 0 0) and a vacant site in position 1(*b*) with coordinates (0 0 1/2). A comparison of the considered structure with that of the high-temperature disordered phase β-W_2C (see Fig. 4 *c*) clearly shows that, as a result of ordering, the positions 2(*a*) one-half of which are randomly occupied by carbon atoms are split into positions 1(*a*) and 1(*b*), where the former are occupied by carbon atoms and the latter remain vacant. At ~2300 K, the homogeneity region of β″-W_2C (α-W_2C) phase extends from $WC_{0.34}$ to $WC_{0.48}$; a decrease in temperature is accompanied by narrowing of this region and, finally, its disappearance at 1523 K and a composition of $WC_{0.48}$ (see Fig. 1). The compositions $WC_{0.41}$ and $WC_{0.50}$ of the β″-W_2C phase have the unit cell parameters $a = 0.2985$, $c = 0.4717$ and $a = 0.3001$, $c = 0.4728$ nm, respectively.[19] If the temperature drops below 1523 K, lower carbide β″-W_2C decomposes to give W and higher carbide δ-WC (WC). Note that later publications provided no information on the rhombohedral (trigonal) [$P\bar{3}m1$ (D^3_{3d})] modification β″-W_2C of lower tungsten carbide with the *C*6-type structure. It cannot be ruled out that the phases β′-W_2C and β″-W_2C described in the literature are in fact the same phase differing in the structures and the degrees of ordering of carbon atoms and vacancies.

Insofar as the X-ray diffraction technique fails to accurately determine the structure of W_2C modifications, neutron diffraction analysis was applied [25–29] in the studies of lower tungsten carbide. W_2C was synthesised by sintering of a pressed powder mixture of tungsten and carbon black (W : C = 2 : 1) at high temperature in vacuum for 3 h; then, the samples were quenched from temperatures of 2670, 2570, 2470 and 2370 K by quick immersion into a bath filled with liquid tin.[25] According to X-ray diffraction data, at 293 K all the samples synthesised had a hexagonal metal sublattice with the parameters $a = 0.2992$ and $c = 0.4721$ nm. The diffraction spectra of W_2C, which were obtained with the use of a monochromatic neutron beam ($\lambda = 0.1131$ nm), revealed, along with structural reflections, weak superstructural reflections which indicated the ordering of carbon atoms and vacancies to form a trigonal ε-W_2C phase which pertains to the ε-Fe_2N structural type. The unit cell parameters of the ε-W_2C phase were found [25] to be $a = a_{L'3}\sqrt{3} = 0.5184$ and $c = c_{L'3} = 0.4721$ nm.

Tungsten carbide samples with the composition ~$WC_{0.43-0.45}$ synthesised by sintering of pressed mixtures of tungsten and carbon black powders at 1920 K for 30–50 h followed by their 10-min cooling to room temperature, were studied.[26] Neutron diffraction analysis has shown that carbon atoms are ordered according to the ε-Fe_2N structural type (*i.e.*, the same type as that reported in Ref. 25). It was found that the ε-W_2C phase has a trigonal structure and pertains to the No. 162 – $P\bar{3}1m$ (D^1_{3d}) space group; the unit cell parameters are as follows: $a = 0.5185$ and $c = 0.4723$ nm. In the ideal trigonal structure of this carbide, all tungsten atoms occupy 6(*k*) positions with coordinates (1/3 0 1/4) and carbon atoms occupy 1(*a*) positions with coordinates c (0 0 0) and 2(*d*) positions with coordinates (1/3 2/3 1/2), while positions 1(*b*) (0 0 1/2) and 2(*c*) (1/3 2/3 0) remain vacant. Figure 4 *d* illustrates the distribution of carbon atoms and vacancies in the non-metal sublattice of ideal trigonal (space group $P\bar{3}1m$) ε-W_2C carbide. However, the best agreement between the experimental and theoretical neutron diffraction patterns was achieved when the population of the positions in the non-metal sublattice by carbon atoms was varied, and a small number of these atoms occupied positions 2(*c*).

Neutron diffraction analysis ($\lambda = 0.1225$ nm) was also used [27] for studying the structure of $WC_{0.45}$ carbide, which was synthesised by the arc fusion of pellets pressed from a mixture of tungsten and carbon powders followed by their quenching to room temperature at a rate of 150 deg s^{-1}. According to the data shown, the studied carbide had the same trigonal (space group $P\bar{3}1m$) crystal structure as in earlier studies;[25,26] the unit cell parameters are $a = 0.5181$, $c = 0.4722$ nm. The best agreement with the experimentally found intensities of reflections (as in Ref. 26) was achieved with allowance made for the different population of non-metal-sublattice sites with carbon atoms; with regard to their population, the sample composition was $WC_{0.42}$. The trigonal structure (space group $P\bar{3}1m$) of the lower carbide ε-W_2C with unit cell parameters $a = 0.5190$, $c = 0.4724$ nm was also revealed;[28,29] a small number of carbon atoms occupied positions 1(*b*) and 2(*c*), which remain completely vacant in an ideal structure of the ε-Fe_2N type.

Thus, neutron diffraction studies [25–29] of lower tungsten carbide samples, which were quenched from the arc fusion temperature [27] and the temperatures of 2670–2370 K (see Ref. 25) and 1920 K,[26] revealed only a trigonal (space group No. 162 – $P\bar{3}1m$) ordered phase with the ε-Fe_2N-type structure. In all the cases, the ordering degree did not reach its maximum. The orthorhombic (space group *Pbcn*) β′-W_2C phase with the Mo_2C-type structure and the rhombohedral (trigonal, space group No. 164 – $P\bar{3}m1$) β″-W_2C phase with the *C*6-type structure were not found by the neutron diffraction analysis.

The temperatures of consecutive phase transformations

$$\beta\text{-}W_2C \rightleftharpoons \beta'\text{-}W_2C,$$

$$\beta'\text{-}W_2C \rightleftharpoons \beta''\text{-}W_2C$$

and eutectoid decomposition

$$\beta''\text{-}W_2C \longrightarrow W + \delta\text{-}WC,$$

namely, ~2750, ~2410 and 1530 K, respectively, were determined [18] using specially designed instruments.[35] The high-temperature differential thermal analysis (DTA) involved [35] a highly sensitive optical (photodiodes and micropyrometer) system for measuring the temperature and the temperature difference between the working and reference samples ΔT. This system allowed one to perform measurements up to 3900 K. With the use of such instruments, the temperatures of phase transformations in hafnium, zirconium and titanium and also in lower carbides of tantalum, molybdenum, and tungsten, *i.e.*, Ta_2C, Mo_2C and W_2C, were determined.[35] Figure 5 *a* shows a DTA curve, which confirms the presence of consecutive transformations of lower tungsten carbide.[18] The authors only noted that all the effects observed at temperature decrease were exothermic. The

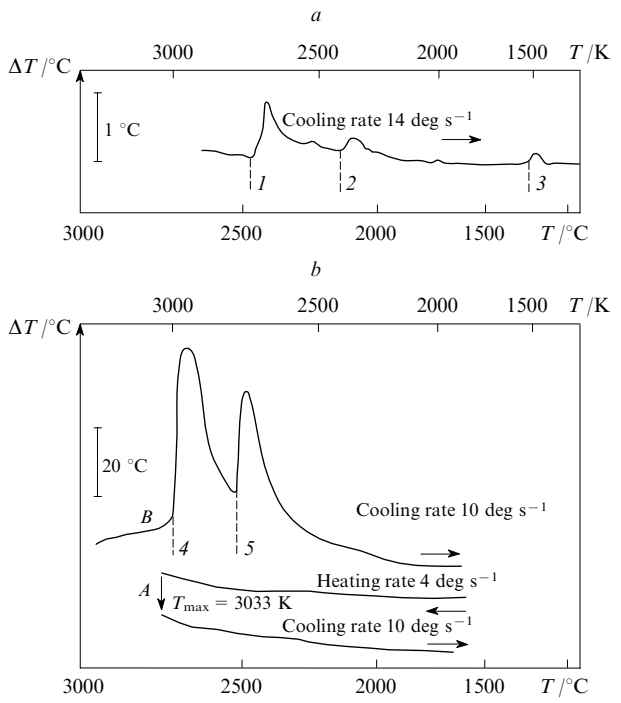


Figure 5. DTA curves of $WC_{0.48-0.49}$ (32.7 at.% of carbon) (*a*) and a carbide containing 51.0 at.% of carbon (*b*).[18,21]
The measurements were carried out on a specially designed set-up (see Ref. 35) which allowed measuring the absolute difference of temperatures ΔT between the standard sample and the sample under study, which depends on the initial experimental conditions; hence, the heat effect can have the opposite sign as compared with the measurements carried out on a standard DTA set-up (the arrows indicate the direction of temperature change);
(*1*–*5*) see text.

small magnitude of thermal effects could be caused by the incomplete transformation due to the too rapid cooling. With allowance made for the results of neutron diffraction studies,[25–29] it is more likely that the effects at ~2750 and 1530 K (positions *1* and *3*), which are observed in the DTA curve, correspond to the transformation

$$\beta\text{-}W_2C \rightleftharpoons \varepsilon\text{-}W_2C$$

and the eutectoid decomposition

$$\varepsilon\text{-}W_2C \rightleftharpoons W + \delta\text{-}WC.$$

The γ-WC_{1-x} phase has a cubic [space group $Fm\bar{3}m$ (O_h^5)] structure of the *B*1 type (NaCl) (Fig. 6), which is typical of all non-stoichiometric carbides and nitrides MX_y of Group IV and V transition metals. The researchers who discovered [30–32] this phase considered it an additional high-temperature phase of lower carbide W_2C. However, based on the theoretical possibility that carbon atoms can occupy all octahedral interstitials in the fcc sublattice of tungsten, it seems more reasonable to consider this phase as a structural modification of higher tungsten carbide. Cubic tungsten carbide was also obtained [32] as a result of the electrospark treatment of tungsten foil, *i.e.*, by generating electric discharge between the foil and a graphite electrode. The existence of cubic WC was confirmed.[22] A phase of γ-WC_{1-x} (β-WC) with the *B*1-type cubic structure was revealed [36] in the products of the plasmochemical synthesis of tungsten carbide; the synthesis was carried out in the argon arc plasma from the tungsten and carbon powders or a tungsten powder and methane. The synthesis with methane gave a product containing from 74% to 96% cubic WC_{1-x} with particles measuring 2–16 nm. No data on the

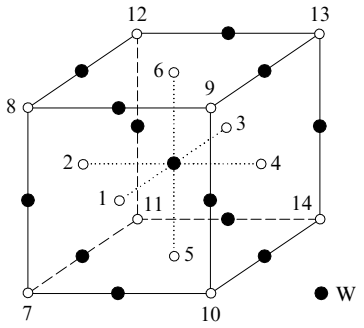


Figure 6. The *B*1-type (NaCl) structure of cubic carbide γ-WC_{1-x}.[1,2] Non-metal sublattice sites are numbered. The first coordination sphere of a tungsten atom in the unit cell centre is formed by sites 1–6 of the non-metal sublattice located in the centres of cell faces; the third coordination sphere is formed by sites 7–14 of the same sublattice, which are located in the cube corners. The second coordination sphere of the central tungsten atom is formed by twelve metal atoms located in the middle of edges.

chemical composition of the obtained cubic phase γ-WC_{1-x} were presented.[36]

Superconducting transition temperature (T_c) for cubic carbides MoC, WC and solid solutions NbC–MoC, NbC–WC, NbC–TaC, TaC–MoC, TaC–WC, MoC–WC with the *B*1 structure were determined.[37,38] Cubic tungsten carbide was synthesised by rapid quenching from the molten state. According to data from Ref. 37, the T_c value is sufficiently high, namely, 10 K for stoichiometric cubic carbide $WC_{1.0}$ and 9 K for cubic $WC_{0.85}$. Yet another sample, which, in addition to the cubic phase, contained lower hexagonal tungsten carbide and a large amount of free carbon, was shown to have T_c = 8.1 K. Assuming that, in the first approximation, the unit cell parameter of cubic WC_{1-x} and its temperature of the superconducting transition depend linearly on the carbon content, then T_c = 8.1 K corresponds to cubic carbide $WC_{0.71-0.72}$ with the unit cell parameter a_{B1} = 0.424 nm. Note that the temperatures of the transition into the superconducting state of hexagonal carbides β-W_2C and δ-WC are 3.6 and 0.3 K, respectively,[37] *i.e.*, substantially lower than those of the cubic phase γ-WC_{1-x}.

It was noted [39] that the electrospark treatment of the molten samples of tungsten carbide and certain WC-based hard alloys produces cubic carbide γ-WC_{1-x}. A cumulative explosion of tungsten, graphite and ammonium nitrate powders allowed the synthesis of samples that contained up to 50 vol.%–70 vol.% γ-WC_{1-x};[40] the explosion conditions were equivalent to those of steady-state sintering at the temperature of 2770–3270 K. Note that in these studies [39,40] cubic carbide γ-WC_{1-x} was designated as β-WC_{1-x}.

According to the phase diagram of the W–C system (see Fig. 1), the single-phase cubic carbide γ-WC_{1-x} exists in the composition range of $WC_{0.58}$–$WC_{0.65}$ at temperatures above 2790–2810 K. Moreover, γ-WC_{1-x} was found in the two-phase regions (β-W_2C + γ-WC_{1-x}) and (γ-WC_{1-x} + δ-WC). The position of the lower boundary of the homogeneity region of cubic carbide γ-WC_{1-x} is independent of the temperature and corresponds to the $WC_{0.59}$ composition;[22] the upper boundary shifts to higher carbon contents with the increase in the temperature and can reach the stoichiometric composition $WC_{1.00}$ (see Fig. 1 *b*). In particular, at 3000–3040 K, cubic carbide γ-WC_{1-x} has a homogeneity region much wider than reported,[19–21] namely, $WC_{0.59}$–$WC_{0.92}$; at ~2800–2810 K, its eutectoid decomposition to β-W_2C and δ-WC (WC) takes place.

Figure 5 *b* shows DTA curves for cubic tungsten carbide containing 51.0 at. % carbon. As is seen, its heating along curves *A* up to ~ 3033 K without any exposure at the maximum temperature failed to melt the sample; its subsequent cooling from 3033 to 1940 K revealed no heat effects. However, curve *B* measured

after the sample was cooled upon its brief exposure at ~3270 K, *i.e.*, from its melt, demonstrates peaks corresponding to strong exothermic heat effects at ~2990 and ~2790–2810 K (positions *4*, *5*). From the viewpoint of the authors,[21] these effects were caused by the following reversible transformations:

the eutectics formation

$$L \rightleftharpoons \gamma\text{-}WC_{1-x} + \delta\text{-}WC,$$

and the eutectoid decomposition

$$\gamma\text{-}WC_{1-x} \rightleftharpoons \beta\text{-}W_2C + \delta\text{-}WC.$$

According to the conditions under which curves *A* and *B* were recorded, cubic carbide γ-WC_{1-x} is formed relatively easily from the melt, but the direct solid-phase transformation

$$\delta\text{-}WC \rightleftharpoons \gamma\text{-}WC_{1-x}$$

is either hindered (for it to happen, the temperature should change slowly near the transformation temperature T_{trans}) or the temperature range of its existence near the stoichiometric composition WC is very narrow.

The phase equilibria in the W–C system were studied [22] in the temperature interval from 2770 to 3100 K (see Fig. 1 *b*) with the use of the X-ray diffraction method, chemical and metallographic analyses and also of the DTA method. To determine the phase composition, the samples heated to 2870 K (or higher) were quenched by cooling to 1800 K in 20 s and lower to 1300 K in 40 s. Samples with the composition between W_2C and WC were quenched from $T \geqslant 2800$ K by their quick immersion into liquid tin with the temperature of 600–650 K. High-temperature DTA was carried out with the use of specially designed (see a patent of Goton [41]) instruments. The temperature interval used in study [22] was narrower than that used by Rudy;[18–21] this is why those phase transitions of lower carbide W_2C, which are associated with its ordering, could not be detected at temperatures below 2750 K.

By and large, the results of independent studies [18–22] on the determination of the temperature and concentration positions of phase boundaries in the W–C system are almost identical. For example, differences between the found phase-transformation temperatures do not exceed 10 K, *i.e.*, they lie within the experimental error range. However, the region of existence of high-temperature cubic monocarbide γ-WC_{1-x} in the phase diagram was studied in more detail.[22] Particularly, a thorough metallographic and X-ray study was carried out for samples quenched from the temperatures above and below 2798 K (the DTA method has shown that a reversible phase transformation takes place at 2798 K in samples containing from 35 at.% to 50 at.% of carbon). Figure 7 illustrates the changes in the microstructures of samples containing 40 at.% of carbon and quenched from 2778 and 2808 K. A sample quenched from 2778 K contained two hexagonal phases W_2C and WC (Fig. 7 *a*). A sample quenched from 2808 K also contained two phases β-W_2C and δ-WC but had a different pearlite-like microstructure (Fig. 7 *b*), which appeared as a result of the eutectoid decomposition of cubic carbide γ-WC_{1-x} formed at $T > 2798$ K. Cubic carbide γ-WC_{1-x} can be directly visualised in the microstructure of samples quenched from higher temperatures (2988–3023 K) in the solid state, and also in the microstructures of samples quenched from the melt from 3043–3063 K (Fig. 8). It was shown [22] that at 3030–3055 K γ-WC_{1-x} has a wide homogeneity region, namely, from $WC_{0.59}$ to $WC_{0.98-1.00}$ (see Fig. 1 *b*).

High temperature of the transition into the superconducting state, namely, 10 K,[37,38] confirms that the composition that corresponds to the upper boundary of the homogeneity region of γ-WC_{1-x} is stoichiometric, *i.e.*, $WC_{1.0}$. It is known [3,4,42] that, among the cubic carbides of Group IV–VI transition metals, stoichiometric carbides $NbC_{1.0}$ and $TaC_{1.0}$ have the highest T_c (10–12 K); however, T_c quickly drops to ~4 K upon their deviation from stoichiometry to $NbC_{0.9}$ or $TaC_{0.9}$ and $T_c \leqslant 1$ K for $NbC_{0.8}$ and $TaC_{0.8}$. According to Willens and Buether,[37] a

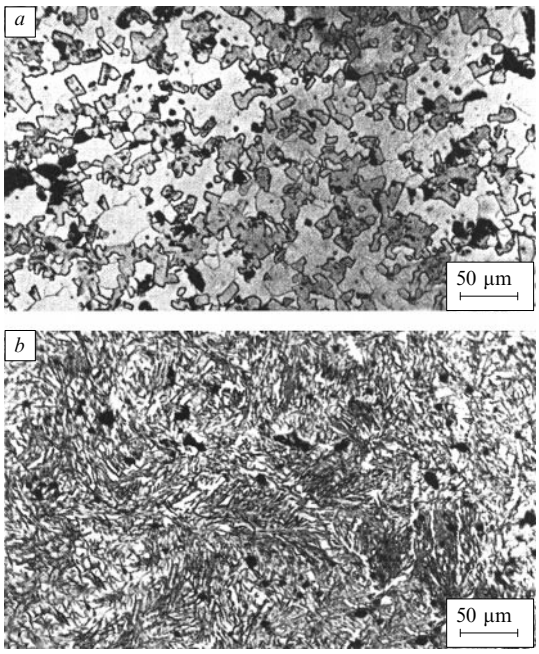


Figure 7. Microstructures of carbide samples with 60 at.% of W and 40 at.% of C quenched from 2778 (*a*) and 2808 K (*b*).[22]
(*a*) The sample contains hexagonal phases of β-W_2C (light grains) and δ-WC (dark grains); (*b*) the sample contains additional phases β-W_2C and δ-WC, but has a pearlite-type microstructure which has appeared at the eutectoid decomposition of cubic γ-WC_{1-x} formed at $T > 2798$ K (see text).

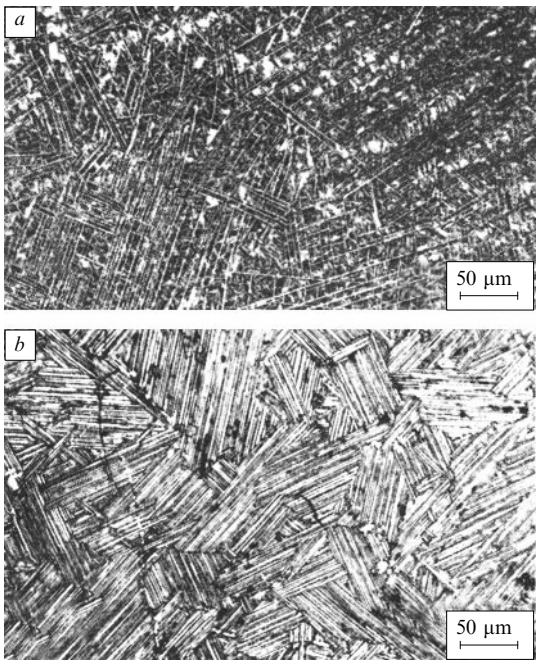


Figure 8. Microstructures of samples with cubic carbide γ-WC_{1-x} obtained by quenching from the melt.[22]
(*a*) A sample with 45 at.% of C quenched from 3043 K contains inclusions of hexagonal monocarbide δ-WC in the matrix of cubic γ-WC_{1-x}; (*b*) eutectic (β-W_2C + γ-WC_{1-x}) microstructure of a sample with 36 at.% of carbon quenched from 3053 K. The sample surface is etched with a 10% NaOH + 30% $K_3Fe(CN)_6$ mixture.

decrease in the carbon content in cubic tungsten carbide causes a relatively smaller decrease in T_c.

The unit cell parameter of γ-WC_{1-x} carbide is $a_{B1} \approx 0.427$ nm;[32] that for cubic carbid $WC_{0.82}$ is $a = 0.4215$ nm.[22] Cubic tungsten carbide with an unknown composition was found to have the unit cell parameter of 0.4229 nm,[36] while almost stoichiometric cubic carbide was shown [39] to have $a = 0.4248$ nm. The unit cell parameters of cubic carbides $WC_{1.0}$, $WC_{0.85}$ and $WC_{0.72}$ were shown [37] to be 0.4266, 0.4252 and 0.4240 nm, respectively. For cubic carbide $WC_{0.61}$, $a = 0.4220$ nm was found;[19,21] the extrapolation of this value to defect-free cubic carbide gave $a = 0.4265$ nm.[43] The unit cell parameter of cubic carbide γ-WC_{1-x} of the unknown composition was found to vary from 0.4222 to 0.4263 nm;[40] such a small unit cell parameter of cubic carbide γ-WC_{1-x} could be caused by oxygen impurity, because the sample was obtained in a cumulative explosion in ammonium nitrate which contains oxygen. The best agreement was observed for the unit cell parameter values found for cubic carbide γ-$WC_{1-x} \equiv \gamma$-WC_y $(y \equiv 1-x)$ [19,21,37–39,43] (Fig. 9). These data are adequately described by a quadratic function

$$a_{B1} = 0.4015 + 0.0481\,y - 0.0236\,y^2 \text{ (nm)}$$

and unambiguously point to the increase in the unit cell parameter of the γ-WC_{1-x} phase with the increase in the carbon content.[44]

Higher tungsten carbide δ-WC (WC) has a negligibly small homogeneity region (or does not have it at all). Its hexagonal [space group $P\bar{6}m2$ (D^1_{3h})] lattice pertains to its own structural type B_h (the WC type) with the unit cell parameters $a = 0.2906$ and $c = 0.2837$ nm.[7,9,10,19] In this structure, tungsten atoms occupy positions 1(a) with coordinates (0 0 0) and carbon atoms are located in positions 1(d) with coordinates (1/3 2/3 1/2).[45] Tungsten and carbon atoms in δ-WC (WC) form simple hexagonal sublattices, in which carbon atoms are located in the centres of trigonal prismatic interstitials of the tungsten sublattice (Fig. 10). The results of simulations of the crystal and electronic structures of hexagonal WC, which were performed [46] by the pseudopotential local-orbital method confirmed the stability of this compound; the estimated unit cell parameters $a = 0.288$ and $c = 0.281$ nm well agree with experimental results.

A positron lifetime study found an experimental confirmation for the stoichiometry of hexagonal monocarbide δ-WC.[47,48] Samples of powder and sintered WC and also samples of a hard WC–Co alloy were studied. The positron lifetime spectra of WC revealed the short-lived ($\tau_{free} = 124 \pm 10$ ps) and more long-lived ($\tau_{\square W} = 175 \pm 20$ ps) components. The former corresponds to the annihilation of positrons from the free state, the latter corresponds to the capture and annihilation of positrons in the metal vacancies the concentration of which is very low. No components

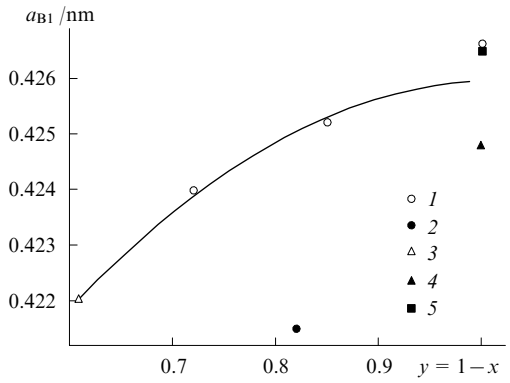


Figure 9. Changes in the unit cell parameter a_{B1} of cubic carbide γ-$WC_{1-x} \equiv \gamma$-WC_y $(y \equiv 1-x)$ with the $B1$-type structure in its homogeneity region.[44]
(*1–5*) The data are taken from Refs 37, 38; 22; 19, 21; 39; 43, respectively.

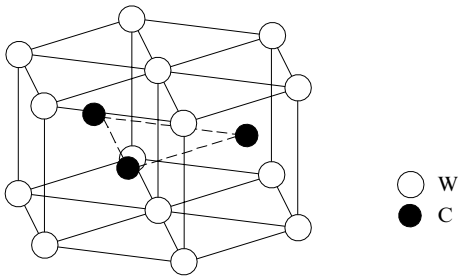


Figure 10. Hexagonal structure of higher carbide δ-WC (WC).

that would correspond to the positron annihilation in the carbon-sublattice vacancies were found. Upon the irradiation of δ-WC with electrons with the energy of 1 MeV, the positron lifetime spectrum contained only one component, namely, with a lifetime of ~136 ps. It was shown [47] that this component corresponds to the capture and annihilation of positrons in the carbon vacancies, which have appeared upon the irradiation. Indeed, the kinetic energy, which is imparted by the 1-MeV electrons to carbon and tungsten atoms in the collisions, is higher than the displacement threshold of the carbon atom from its position but lower than the displacement threshold of the tungsten atom; hence, the vacancies were induced only in the carbon sublattice of the carbide. Due to the higher imparted energy, the irradiation of δ-WC with electrons with the energy of 2.5 MeV resulted in the displacement of both carbon and tungsten atoms and the appearance of vacancies in both sublattices.[48] A comparison of the experimental results [47,48] with those obtained in the calculations of the positron lifetime by the method of linear muffin-tin orbitals in the atomic sphere approximation (LMTO-ASA) [49] in a model carbide WC with the cubic $B1$-type lattice demonstrated good agreement of calculations with experimental data for $\tau_{\square W}$ in a metal vacancy and a noticeable deviation in the positron lifetime $\tau_{\square C}$ in a carbon vacancy. On the whole, the results [47,48] confirmed that, under normal conditions, higher hexagonal carbide δ-WC is stoichiometric and has no carbon vacancies in its carbon sublattice.

Thus, among tungsten carbides, only higher hexagonal carbide δ-WC (WC) has virtually no homogeneity region, whereas lower carbides W_2C and cubic γ-WC_{1-x} have relatively wide homogeneity regions. Table 1 gives information on the crystal structures of the phases in the W–C system. It should be borne in mind that the conclusions made in those studies in which the structures of non-stoichiometric tungsten carbides were determined only based on the X-ray diffraction data are merely the assumptions. Particularly, this concerns W_2C, the non-metal sublattice of which was assumed ordered with respect to both atoms and vacancies. The structures of non-stoichiometric tungsten carbide compounds found by the neutron diffraction analysis are more confident and reliable.

The main difference between the phase diagrams of the W–C system proposed by Rudy *et al.*,[19–21] on the one hand, and Sara,[22] on the other hand, concerns the position and width of the homogeneity region of cubic carbide γ-WC_{1-x}. The authors of the former studies [19–21] were short of experimental results sufficient to determine the position of this carbide in the phase diagram and had to use the analogy with the Mo–C system studied earlier.[50,51] Thus, having detected the β-MoC_{1-x} (Mo_3C_2 or $MoC_{0.67}$) phase with a narrow homogeneity region, they assumed that the WC_{1-x} phase in the W–C system has the same stoichiometric composition W_3C_2 ($WC_{0.67}$) and the equally narrow homogeneity region.§

§ It is not by accidence that the paper by Rudy *et al.*,[19] in which the version of the phase diagram of the W–C system presented in Fig. 1 *a* was published, was entitled 'W–C System: supplemental information on the Mo–C system'.

Table 1. Crystal structure of phases that can exist (according to different authors) in the W–C system at $T > 1300$ K.

Phase		Existence region (at.% of C)	Unit cell parameters /nm			Space group	Pearson symbol	Lattice type and symmetry
designations as in Fig. 1 (data from Ref. 17)	designations in other studies		*a*	*b*	*c*			
W	W	0–1.0	0.3165			$Im\bar{3}m$ (O_h^9)	*cI*2	*A*2 (W type), bcc
β-W_2C	γ-W_2C (see [a])	~25.5–34.0	0.3002		0.475–0.476 (see [b])	$P6_3/mmc$ (D_{6h}^4)	*hP*3	*L*′3 (W_2C type), hexagonal
β′-W_2C	β-W_2C (see [a])	~29.5–33.0	0.4728	0.6009	0.5193 (see [c])	$Pbcn$ (D_{2h}^{14})	–	PbO_2 or Mo_2C (ζ-Fe_2N) type, orthorhombic
β″-W_2C	α-W_2C (see [a])	~29.5–32.5	0.2985 (see [d]) 0.3001 (see [e])		0.4717 (see [d]) 0.4728 (see [e])	$P\bar{3}m1$ (D_{3d}^3)	*hP*3	*C*6 (*anti*-CdI_2 type), rhombohedral
	ε-W_2C (see [f])	~29.5–33.0 (at $T \approx 2500$ K)	0.5184		0.4721 (see [f])	$P\bar{3}m1$ (D_{3d}^1)	–	ε-Fe_2N type, trigonal
γ-WC_{1-x}	α-WC_{1-x} (see [g]) β-WC (see [i])	~37.0–39.5 (see [g]) ~37.1–50.0 (see [j])	0.4265 (see [h]) 0.4252 (see [k])			$Fm\bar{3}m$ (O_h^5)	*cF*8	*B*1 (NaCl type), cubic
δ-WC	WC (see [g]) α-WC (see [j])	~50	0.2906		0.2837 (see [b])	$P\bar{6}m2$ (D_{3h}^1)	*hP*2	B_h (WC type), hexagonal
C	C	100	0.142		0.339	$P6_3/mmc$ (D_{6h}^4)	*hP*4	*A*9 (C, graphite), hexagonal

Note. In the study,[17] the phase diagram of the W–C system takes into account the structural data,[18–22, 34] some of which were not confirmed later; trigonal (space group $P\bar{3}1m$) ε-WC phase the existence of which was reliably confirmed [25–29] is not shown in the phase diagram of the W–C system (see Ref. 17). Here and in Table 2, the γ-WC_{1-x} phase is identical to the γ-WC_y ($y \equiv 1-x$) phase.
[a] Refs 18, 21; [b] Ref. 19; [c] Ref. 18; [d] Ref. 19 for $WC_{0.41}$; [e] Ref. 19 for $WC_{0.50}$; [f] Ref. 25; [g] Ref. 21; [h] Ref. 43 for $WC_{1.0}$; Refs 22, 36; [j] Ref. 22; [k] Ref. 31 for $WC_{0.85}$.

At the same time, it follows from the study by Sara [22] that the homogeneity region of cubic γ-WC_{1-x} is much wider than that given in Refs. 19–21 and reaches the $WC_{1.0}$ composition, which agrees with the results of later studies (see Refs 32, 36–39). However, for a cubic carbide of the stoichiometric composition $WC_{1.0}$, the phase diagram (see Fig. 1 *b*) [22] contains no temperature region of its existence, while the region of the existence of the γ-WC_{1-x} has such boundaries at $(1-x) \to 1$ that the temperature decrease merely from 3058 to 3028 K causes the following consecutive transformations in the $WC_{1.0}$ composition: first, a peritectic transformation and then a peritectoid one. This is highly improbable. Moreover, the line of phase equilibrium *1–2–3* (see Fig. 1 *b*) is shown incorrectly in the cited study, namely, from a horizontal that corresponds to the non-variant eutectic process

$$L \rightleftharpoons \beta\text{-}W_2C + \gamma\text{-}WC_{1-x},$$

this line gradually transforms into a monovariant curve, which is physically impossible and incorrect from the viewpoint of thermodynamics. The phase equilibrium shown could be possible if point *2* was a singular point, *i.e.*, a kink point. However, this in turn, would have led to the narrowing of the temperature interval of the existence of a two-phase region L + γ-WC_{1-x} and to the shift of its lower boundary to higher temperatures, which contradicts the DTA results.[22] If a cubic carbide with the stoichiometric composition $WC_{1.0}$ had at least a narrow temperature range of stability and the two consecutive phase transitions were somewhat shifted in the composition with respect to one another, then the noted inaccuracies and contradictions could be eliminated and the total body of experimental results could be taken into account.

Figure 11 shows the phase diagram of the W–C system, which was constructed [44] with allowance made for the presence of the temperature interval of existence of cubic carbide $WC_{1.0}$ and also for experimental results [18–22, 32, 36–39] and the results of new structural and magnetic-susceptibility studies of tungsten carbides synthesised in our studies. It is evident that, in the temperature range of 3058–2993 K, in the vicinity of the $WC_{1.0}$ composition, a decrease in temperature results first in the peritectic formation of cubic tungsten carbide from the melt

$$L + C \rightleftharpoons \gamma\text{-}WC_{1-x},$$

and then in the transformation of cubic monocarbide into the hexagonal modification

$$\gamma\text{-}WC_{1-x} \rightleftharpoons \delta\text{-WC}.$$

The temperature of the eutectoid decomposition

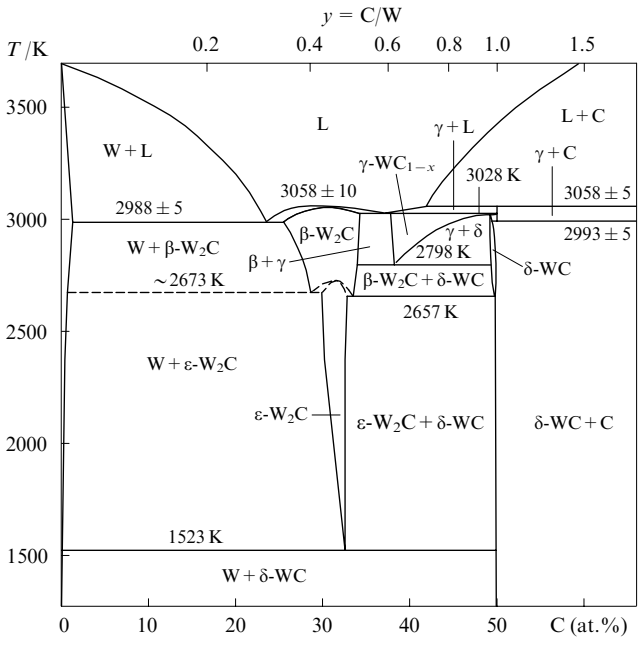


Figure 11. Phase diagram of the W–C (γ-$WC_{1-x} \equiv$ γ-WC_y) system [44] with corrected positions of phase boundaries in the region of lower tungsten carbide W_2C. Corrections were introduces according to the neutron diffraction results [25–29] (see text).

Table 2. Special points in the phase diagram of the W – C system (Fig. 11) at a temperature above 1300 K (according to Ref. 44 with corrections made in the region of the existence of lower tungsten carbide W_2C).

Reaction	Composition of phases involved in the reaction (at.% of C)			T /K	Reaction type
$L \rightleftharpoons W$	0	0	–	3755 ± 5	melting
$L \rightleftharpoons \beta\text{-}W_2C$	~30.6	~30.6	–	3058 ± 10	congruent melting
$L + C \rightleftharpoons \gamma\text{-}WC_{1-x}$	~42.0	100.0	50.0	3058 ± 5	peritectics
$L \rightleftharpoons W + \beta\text{-}W_2C$	~23.5	~1.2	~25.5	2988 ± 5	eutectics
$L \rightleftharpoons \beta\text{-}W_2C + \gamma\text{-}WC_{1-x}$	~37.0	~34.3	~37.8	3028 ± 5	"
$\gamma\text{-}WC_{1-x} \rightleftharpoons \delta\text{-}WC$	~49.3	~49.3	–	3008 ± 5	polymorphic transformation
$\gamma\text{-}WC_{1-x} \rightleftharpoons \delta\text{-}WC + C$	50.0	~49.8	100.0	2993 ± 5	eutectoid decomposition
$\gamma\text{-}WC_{1-x} \rightleftharpoons \beta\text{-}W_2C + \delta\text{-}WC$	~38.2	~34.0	~49.5	2798 ± 5	the same
$\beta\text{-}W_2C \rightleftharpoons W + \varepsilon\text{-}W_2C$	~28.6	~0.7	~29.7	2673 ± 10	"
$\beta\text{-}W_2C \rightleftharpoons \varepsilon\text{-}W_2C$	~31.6	~31.6	–	2728 ± 10	disorder – order transformation
$\beta\text{-}W_2C \rightleftharpoons \varepsilon\text{-}W_2C + \delta\text{-}WC$	~33.5	~32.8	~49.8	2657 ± 10	eutectoid decomposition
$\varepsilon\text{-}W_2C \rightleftharpoons W + \delta\text{-}WC$	~32.6	0	50.0	1523±5	the same

$$\gamma\text{-}WC_{1-x} \rightleftharpoons \delta\text{-}WC + C,$$

equal to 2993 K (see Fig. 11) was found from the results of DTA [21] for a sample with 51 at.% carbon. This value was assigned to the temperature of the eutectic [21]

$$L \rightleftharpoons \beta\text{-}W_2C + \gamma\text{-}WC_{1-x}.$$

However, even according to the phase diagram version proposed,[21] such a carbide composition falls beyond a region where this phase equilibrium is permitted. Therefore, this temperature cannot be the temperature of the eutectic. Although the temperature interval of the equilibrium existence of $\gamma\text{-}WC_{1-x}$ (see Fig. 11) is small, the cubic carbide of the stoichiometric composition $WC_{1.0}$ can at least be quenched from the melt, which agrees with the experimental results.[37, 38]

The phase diagram W – C published in study [44] contains the following corrections in the positions of phase boundaries in the lower tungsten carbide W_2C region, which were introduced with allowance made for the neutron diffraction results:[25–29] the $\varepsilon\text{-}W_2C$ phase is shown in place of phases $\beta'\text{-}W_2C$ and $\beta''\text{-}W_2C$, the existence of which is not confirmed experimentally. These corrections are reflected in Fig. 11. The special points in the phase diagram of this system at temperatures above 1300 K are described in Table 2.

III. Phase equilibria in the W – Co – C system

The wide application of high-strength hard alloys formed in the pseudobinary system WC – Co brought about the investigations of the phase equilibria in the ternary system W – Co – C.

Information on the phases in the W – Co – C system which was obtained before 1952 is generalised in a review,[52] where new diffraction, metallographic and DTA studies of this system were carried out. In addition, the liquidus surface projection, the total isothermal cross-section at 1673 K and the pseudobinary *c vs. T* diagrams along the cross-sections C – $Co_{43}W_{57}$ and WC – Co were constructed, in which the stable and metastable phase equilibria were specified. In the pseudobinary cross-section WC_y – Co (16 mass % of Co), the effect of the carbon content on the phase equilibria and structure of alloys was studied.[53] The results of the metallographic and diffraction studies of the M_6C-type cubic η-carbides, which are formed in the W – Co – C system, were discussed.[54] Particularly, η-carbide Co_2W_4C with a cubic cell parameter, which varied from 1.107 to 1.125 nm depending on the carbon content, was revealed; two total isothermal cross-sections of the W – Co – C system were constructed at temperatures 1273 and 1673 K. The stability of η-carbides of the M_6C type in the W – Co – C system was also considered by other authors [55] who showed additional isothermal cross-sections in this system at 1373 and 1573 K. The experimental studies of phase equilibria in the W – Co – C system at 1423 K were supplemented by thermodynamic calculations.[56]

According to the results of numerous studies, the system W – Co – C forms several ternary compounds, *viz*., cubic [space group $Fd\bar{3}m$ (O_h^7)] η-carbides Co_2W_4C (see Ref. 54) and Co_4W_2C (see Ref. 57) of the M_6C type and also two hexagonal [space group $P6_3/mmc$ (D_{6h}^4)] CoW_3C carbides with the $Co_3W_9C_4$ (see Ref. 58) and $Co_6W_{20}C_7$ structures.[59] Note that the $Co_3W_9C_4$ structure has two types of metal sublattice interstitials, in which carbon atoms are located as follows: in the unit cell, two carbon atoms of eight are located in the centre of trigonal prisms formed by six tungsten atoms, while the remaining six carbon atoms are in the centres of octahedra formed of five tungsten and one cobalt atoms. A comprehensive study of these carbides showed that all of them can exhibit a noticeable carbon deficiency, *i.e*., they are non-stoichiometric; hence, their compositions should be written with allowance made for the possible non-stoichiometry, namely, $Co_2W_4C_y$, $Co_4W_2C_y$ and CoW_3C_y. Carbides $Co_2W_4C_y$ and $Co_4W_2C_y$ are often united into a single phase $Co_3W_3C_y$. It is evident that here we have a pseudobinary solid solution between $Co_2W_4C_y$ and $Co_4W_2C_y$. For the case of deficient carbon content, this variable-composition phase corresponds to the $\sim Co_6W_6C_y$ carbide in the phase diagram.

The results of the aforementioned studies are taken into account in a comprehensive survey,[60] which is devoted to the thermodynamic properties and phase equilibria in the W – Co – C system; moreover, the author of this survey carried out calculations to refine the phase equilibria by means of the CALPHAD method (see Ref. 61) using the approximations and models described elsewhere.[62] Figure 12 shows a series of isothermal cross-sections of the ternary system W – Co – C at 2073, 1773, 1698, 1673, 1548 and 1443 K, which were constructed based on these calculations and are shown in a handbook.[63] All isothermal cross-sections contain carbide of the $\sim Co_6W_6C$ composition and a solid solution $Co_3W_3C_y$ [in the survey cited (Ref. 60), they appear as $M_{12}C$ and M_6C, respectively]. In the isothermal cross-section at 1273 K, the solid solution $Co_3W_3C_y$ is absent but a η-carbide Co_2W_4C appears.[60] As is seen, the ternary compounds are formed where the carbon content in an alloy is lower than the tungsten content. Note that the isothermal cross-section of the W – Co – C system at 1273 K ignores the existence of the hexagonal intermetallic phase Co_3W, which stabilises at $T \leqslant 1350$ K and decomposes *via* the peritectoid reaction at ~1360 K.

Figure 13 shows a section of the ternary system W – Co – C cut along the WC – Co plane. This section contains two- and three-phase regions. In this system, the liquid phase appears at 1560 – 1593 K. According to the survey cited (Ref. 60), the maximum solubility of WC in solid cobalt does not exceed

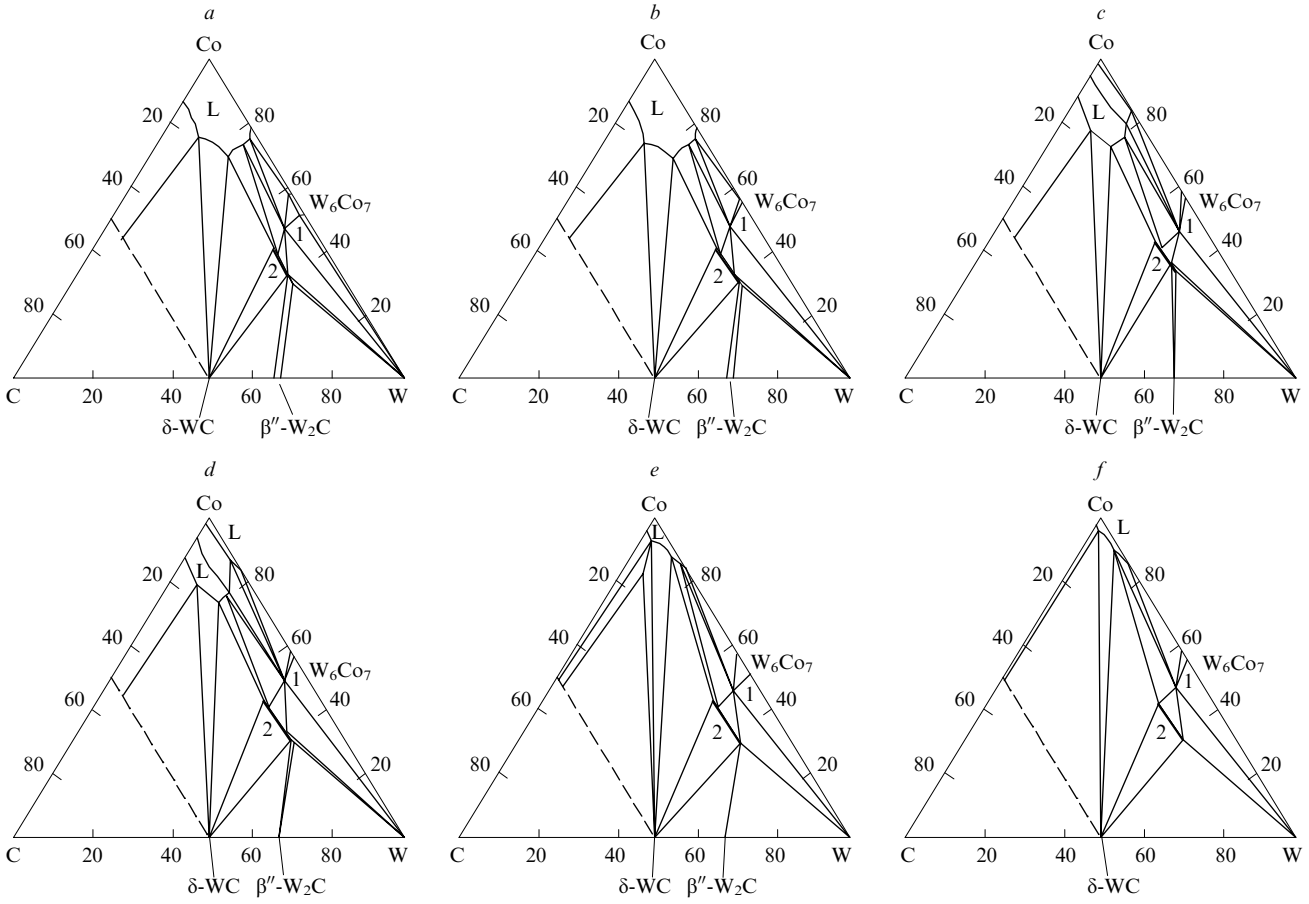


Figure 12. Isothermal cross-sections of the ternary W–Co–C system at 2073 (*a*), 1773 (*b*), 1698 (*c*), 1673 (*d*), 1548 (*e*) and 1443 K (*f*).[63]
The concentrations are shown in at.%, the triple point position corresponds to the results of thermodynamic calculations;[60] (*1*) $Co_6W_6C_y$, (*2*) $Co_3W_3C_y$.

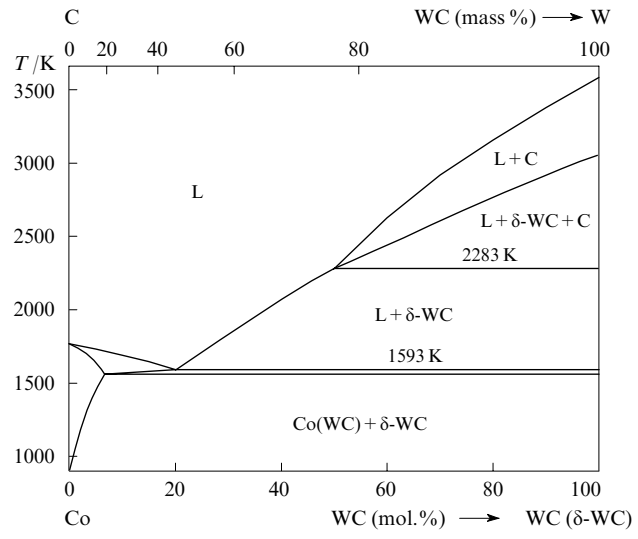


Figure 13. Section of the ternary W–Co–C system cut along the WC–Co plane.[60]

6.7 mol.% (or 19.3 mass %); as the temperature decreases to 1270 K, the solubility does not exceed 3 mol.% (~9 mass %). According to the earlier data (see Ref. 7, vol. 1, p. 262), the maximum solubility of WC in cobalt reaches 22 mass %. A solid solution of WC in cobalt Co(WC) is formed as a result of the diffusion dissolution and appears when the sintering temperature of the WC–Co system reaches 1420–1570 K. A part of cobalt which does not belong to the solid solution composition passes into the liquid phase that wets the carbide grains.

IV. Electronic structures of tungsten carbides

The band structures of hexagonal and cubic carbides W_2C and WC were calculated.[46, 64–68] The electronic structure of hexagonal carbide WC was calculated [64] by a non-self-consistent method of augmented plane waves (APW). A more correct investigation of the band structure in the bulk and on the surface of hexagonal carbide WC was performed by a self-consistent linear method of augmented plane waves (LAPW).[65]

Figure 14 *a* shows the calculated curve of the density of electronic states for hexagonal WC. The Fermi level is located near the curve minimum, and the density of electronic states on this level is relatively low, *viz*., approximately 0.34 eV^{-1} (~4.6 Ry^{-1}) per unit cell. The Fermi surface of hexagonal WC has small hole and electron 'pockets' in the vicinity of *K* and *L* sites of the Brillouin zone.[65]

The electronic structure of hexagonal WC was calculated [46] by the pseudopotential local-orbital method. Figure 14 *b* shows the resulting curves of the density of electronic states [it is the density of spin states $N_{sp}(E)$ that was calculated; to make the comparison easier, the figure shows the density of electronic states $N(E) = 2N_{sp}(E)$ in place of the density of spin states]. It is evident that the calculated [46, 65] density-of-states curves of hexagonal WC are in adequate agreement with one another, *viz*., the Fermi level is located in a distinct density-of-states minimum and the quantity $N(E_F)$ is ~0.3 eV^{-1} per unit cell. Presumably,[46, 65] it is the small density of electronic states on the Fermi level that determines the high stability of this carbide. The low temperature of the WC

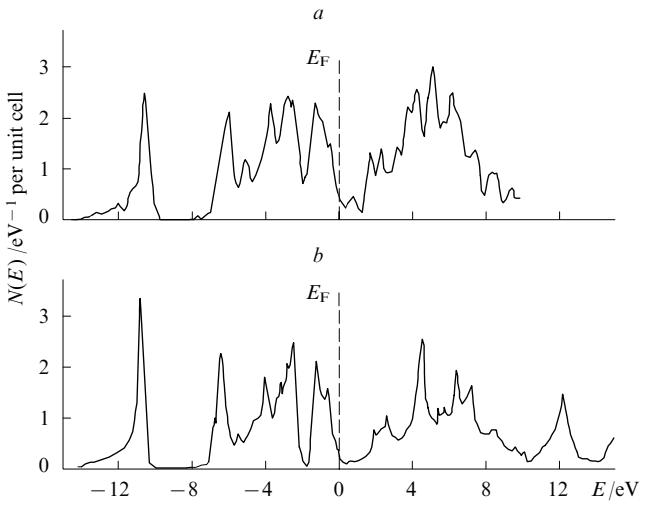


Figure 14. Curves of the total density of electronic states $N(E)$ for hexagonal (space group $P\bar{6}m2$) tungsten monocarbide.
(*a*) LAPW calculations;[65] (*b*) calculations by the pseudopotential local-orbital method.[46]

transition into the superconducting state [$\sim$1.3 K (see Ref. 69)] was also associated [46] with the low $N(E_F)$.

The linear method of muffin-tin orbitals in the atomic sphere approximation (LMTO-ASA) used for calculation [66] of the densities of states not only for higher hexagonal tungsten carbide, but also for cubic (*B*1-type structure) monocarbide WC [as was shown above (see Section II), to date, non-stoichiometric cubic carbide WC_y with $y \leqslant 0.82$ is experimentally detected, although the upper boundary of the homogeneity region of cubic tungsten carbide approaches $WC_{1.0}$]. Figure 15 shows the calculated curves of the density of states $N(E)$.

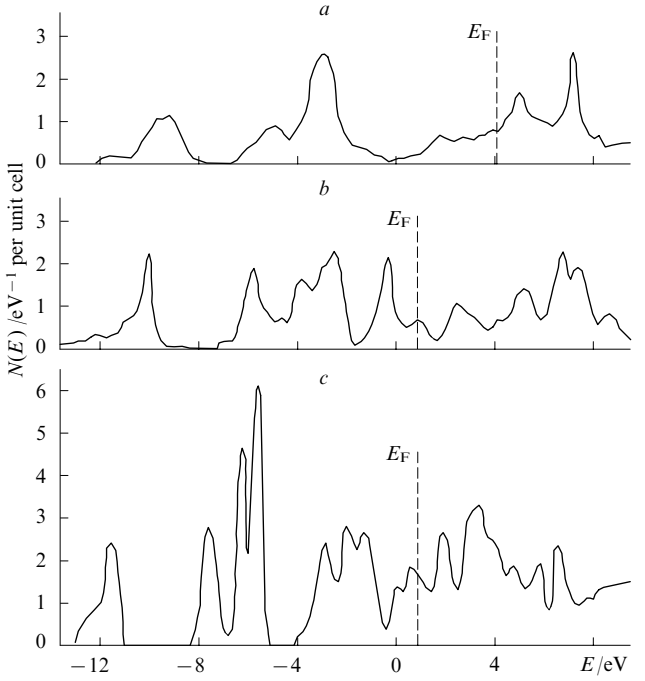


Figure 15. Curves of density of electronic states $N(E)$ of tungsten carbides in the LMTO-ASA approximation.[66]
(*a*) Hexagonal monocarbide WC (space group $P\bar{6}m2$), (*b*) cubic monocarbide WC (space group $Fm\bar{3}m$, *B*1-type structure), (*c*) lower hexagonal carbide W_2C (space group $P6_3/mmc$).

The curves of the density of electronic states $N(E)$ for hexagonal WC, which are shown in Figs 14 and 15 *a*, differ, first of all, in the Fermi level position. According to calculations,[66] the Fermi level of this carbide is located in a band formed largely by the 5d states of tungsten, and $N(E_F) = 0.78$ eV^{-1} per unit cell (10.6 Ry^{-1}), *i.e.*, almost twice greater than it follows from other calculations.[46, 65] Note that in their later publication,[67] the authors of a study [66] showed a different density-of-states curve of hexagonal WC, which is closer to those calculated in the studies [46, 65] and has the Fermi level in a different position near the $N(E)$ minimum and also a lower $N(E_F)$ value.

The curve of the density of electronic states for cubic WC (Fig. 15 *b*) is on the whole similar to the corresponding curves of cubic carbides of other transition metals MC (M = Ti, Zr, Nb, Ta) and contains a low-energy 2s(C) band with small contributions of s, p and d states of tungsten, a ground-state valence-binding band formed due to the hybridisation of 2p(C) and 5d(W) states and a high-energy band largely formed by the 5d(W) states with an admixture of 6s(W) states. As compared with the $N(E)$ curve of TaC carbide (a typical non-stoichiometric carbide, the closest to WC), the 2s(C) and 2p(C) – 5d(W) bands of the cubic tungsten carbide are somewhat broadened due to the smaller WC unit cell parameter.

The band structure of W_2C is intermediate between the band structure of bcc metallic tungsten and hexagonal WC. The main difference in the density-of-states curves of hexagonal W_2C (Fig. 15 *c*) and hexagonal and cubic monocarbides (see Fig. 15 *a*,*b*) is that W_2C has narrower bands; hence, the hybridised valence-binding and metal 5d(W) bands have the density of states much higher as compared with monocarbides WC. The density of electronic states at the Fermi level is also higher for W_2C as compared with higher hexagonal and cubic WC, namely, the $N(E_F)$ values calculated [66] per unit cells of hexagonal and cubic WC and also for lower hexagonal carbide W_2C are 0.78, 0.86 and 2.17 eV^{-1} (10.6, 11.7 and 29.5 Ry^{-1}), respectively.

Based on the results of band structure calculations, the unit cell parameters, the compression bulk modulus B (also conventionally designated as K) and the Debye temperature θ_D were calculated for these carbides. The modulus of elasticity of hexagonal WC is 655 GPa (6.55 Mbar), which substantially exceeds that of lower carbide W_2C (490 GPa).[66] For hexagonal WC, the same authors showed a different calculated value of modulus of elasticity equal to 699 GPa (Ref. 67). The B values are 60% – 70% higher than the value 413 GPa (4.13 Mbar) found for the same carbide.[46] The lowest bulk compression modulus equal to 375 GPa, was obtained [66] for cubic WC; the unit cell parameter a_{B1} was calculated to be 7.98 a.u. (0.422 nm). The small modulus of elasticity of this carbide is associated with its metastable state, because the energy of valence electrons in cubic WC is higher than that in hexagonal carbide by $\sim$12.2 eV ($\sim$0.9 Ry).[5, 66, 68]

As noted above, the measurements of the positron lifetime allowed the vacancies to be revealed in the carbon and metal sublattices of irradiated hexagonal carbide WC.[47] Taking into account this experimental result, an attempt was undertaken [70] to elucidate how the metal and carbon vacancies affect the WC band structure. The calculations were performed using a self-consistent *ab initio* total potential method (LMTO-TP). The simulations of stoichiometric and defective carbides involved the use of a supercell formed by eight tungsten-sublattice and eight carbon-sublattice sites which are occupied according to the stoichiometries W_8C_8 (WC), W_8C_7 ($WC_{0.875}$) and W_7C_8 ($W_{0.875}C$). Figure 16 shows the calculated [70] total density of electronic states for tungsten carbides. According to earlier calculations,[46, 65–68] the valence band of the hexagonal stoichiometric monocarbide consists of two subbands separated by a forbidden gap. The lower subband A is largely formed by states 2s(C), while the subband B of a larger energy is formed by states 2p(C) – 5d(W), *i.e.*, is hybridised. The Fermi level [$E_F = 25.3$ eV, $N(E_F) = 0.23$ eV^{-1} per unit cell] is located near the minimum of the density-of-states curve (Fig. 16 *a*). Upon the introduction of a carbon vacancy, a

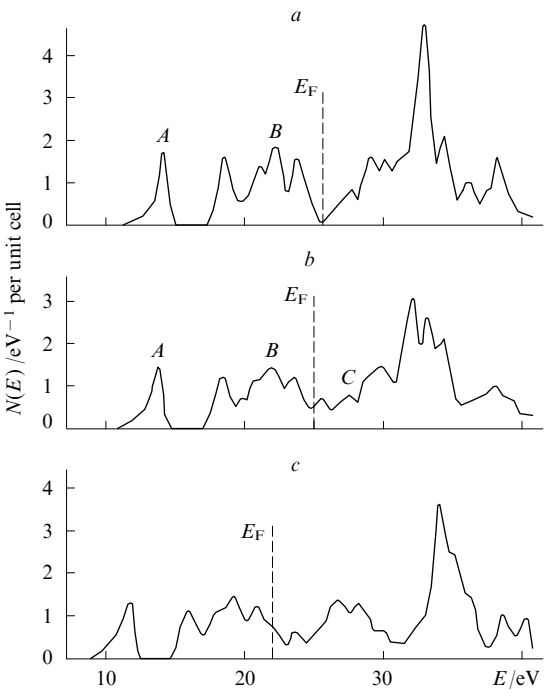


Figure 16. The effect of vacancies on the total density of electronic states $N(E)$ of hexagonal tungsten carbide according to LMTO-TP calculations.[70]
(*a*) Stoichiometric carbide WC, (*b*) carbide $WC_{0.875}$ (W_8C_7) with carbon vacancies, (*c*) carbide $W_{0.875}C$ (W_7C_8) with vacancies in the tungsten sublattice.

vacancy peak *C* appears a little higher than the Fermi level, the density of states on the Fermi level $N(E_F)$ increases up to 0.61 eV^{-1} per unit cell and the band *B* acquires its fine structure (Fig. 16 *b*). The presence of a vacancy in the tungsten sublattice also results in both the appearance in the Fermi level vicinity of a small vacancy peak and the increase in $N(E_F)$ up to 0.69 eV^{-1} per unit cell (Fig. 16 *c*). The introduction of a carbon or a tungsten vacancy reduces E_F to 25.0 and 22.0 eV, respectively. The calculated[70] distribution of electronic density in the spheres of the tungsten and carbon vacancies and the charges of these vacancies ($q_{\square C} = 0.67$e, $q_{\square W} = 0.51$e) are in qualitative agreement with the positron lifetime in these vacancies:[47] the charge of a carbon vacancy is higher, hence, the positron lifetime in it is shorter as compared with the vacancy in the tungsten sublattice ($\tau_{\square C} = 136$ and $\tau_{\square W} = 175$ ps, respectively).

According to the results of calculations,[46, 64–68, 70] the band structure of studied tungsten carbides is basically the same, *viz*., it contains three main bands, namely, the low-energy 2s(C) band, the ground-state hybridised valence binding band 2p(C)–5d(W) and the high-energy band formed largely by the 5d states of tungsten.

V. Methods of synthesis of tungsten carbides and WC–Co alloys with different grain sizes

Polycrystalline metal carbides are usually synthesised by the powder metallurgy methods, which are described in detail in monographs.[3, 4] Different synthetic methods are also described.[71–73] The most popular methods are those that involve the direct synthesis from a metal and carbon or from the compounds containing the metal (for example, metal oxides or chlorides) and carbon (*e.g*., a hydrocarbon or CO).

A conventional method of the synthesis of hexagonal carbide WC involves heating of tungstic acid (H_2WO_4) or ammonium tungstate $(NH_4)_2WO_4$ in a mixture of hydrogen and methane at 1020–1270 K. When tungstic acid is used, the metal is completely reduced even before the carburisation. The carbothermal reduction of WO_3 by carbon in the inert or reductive atmosphere proceeds in a similar way. Tungsten carbide synthesised by carbothermal reduction usually contains traces of oxygen and oxycarbides; therefore, synthesis of a pure substance requires that the latter be additionally annealed at a temperature not lower than 1800 K.

The purest hexagonal WC samples are synthesised by the solid-phase vacuum sintering of metallic tungsten and carbon (gas black) at a temperature not lower than 1400 K. Hexagonal carbide W_2C is synthesised by the solid-phase vacuum sintering of tungsten and carbon powders at 850–900 K. However, the solid-state carburisation at this low temperature proceeds only in the presence of hydrogen or a gaseous hydrocarbon; moreover, the final product contains a relatively high amount of free carbon. Synthesis of a single-phase WC powder with the grain size of 5–6 μm from the metallic tungsten powder in a mixture of hydrogen with methane has been described;[74] at 2300–2500 K and a gas mixture with $\leqslant 2$ vol.% of methane, WC with the free carbon content < 0.1 mass % could be obtained. High temperature (up to ~ 2400 K) is required in those cases where the solid-state sintering is carried out in vacuum, although the carburisation starts at 1400 K.

Tungsten carbides can also be synthesised using the following methods: deposition from the gas phase in the reaction of $W(CO)_6$ or tungsten chloride with a mixture of a hydrocarbon and hydrogen, thermal decomposition of various precursors,[75] self-propagating high-temperature synthesis and mechanochemical synthesis.[76] For example,[77] a mixture of carbon (black) and tungsten powder with the grain size of up to 10 μm was ground in a cam-type mill; during the grinding, the average load in the ball impact zone was 10^8–10^9 Pa and the quantity of mechanical energy absorbed by the powder during the grinding reached 30 kJ g^{-1}. As a result of such treatment, lower hexagonal tungsten carbide was obtained. Mechanosynthesis of carbides from elementary tungsten and carbon in a planetary ball mill with the use of an inert copper matrix was described;[78] according to authors' estimates, the average size of W_2C and WC particles formed did not exceed 0.5 μm.

We have already mentioned that hexagonal carbide WC is not the hardest and most refractory among carbides. Its melting point (~ 3060 K) is lower as compared with TiC, ZrC, HfC, NbC and TaC, and its hardness at 300 K (according to different sources, from 18 to 22 GPa) is lower as compared with non-stoichiometric carbides TiC_y, ZrC_y, HfC_y, VC_y, NbC_y, TaC_y at the same temperature.[3, 4] However, the hardness of WC is sufficiently stable, *e.g*., as a result of carbide heating from 300 to 1300 K, the microhardness H_V of hexagonal WC decreased from ~ 18 to ~ 12 GPa,[79] whereas H_V of carbides of other metals decreased under the same conditions from their maximum values to 3–8 GPa (Fig. 17). The increase in temperature from 300 to 1100 K is accompanied by a more pronounced decrease (approximately three-fold) in the WC hardness; however, the hardness of other carbides undergoes a still sharper decrease (approximately five-fold) in the same temperature range.[80] The sharp decrease in the WC hardness with the increase in the temperature follows from the experimental results,[81] which, nonetheless, substantially differ from those given by other authors[79, 80] (the same study[81] also shows the hardness value for vanadium monocarbide at ~ 900–1500 K, which is lower as compared with that found in other literature sources). Apparently, the value of WC hardness measured in the study cited (Ref. 81) is severely underestimated. Moreover, note that, as compared with other carbides, WC has a modulus of elasticity higher by a factor of 1.5–2 [~ 700 GPa (see Ref. 82)] and a thermal expansion coefficient lower by a factor of 1.5 [$(5-6) \times 10^{-6}$ K^{-1} (see Ref. 82)].

The mentioned properties of WC and their temperature stability during the heating up to 900–1000 K determined its application as the basis of wear-resistant hard alloys that are used in metal-working and drilling operations. The direct use of WC for

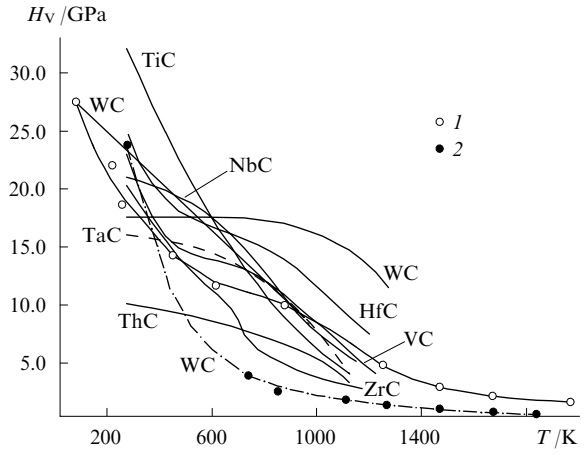


Figure 17. The effect of temperature on the Vickers hardness of hexagonal WC and carbides of transition metals.[79]
For comparison, the known $H_V(T)$ dependences of monocarbide WC (*1*)[80] and (*2*)[81] are shown (see text).

these purposes is impossible because of its brittleness and sintering only at very high temperatures. Hence, for a given carbide to be applied in practice, it should be imparted certain viscosity without sacrifice in its hardness. This is achieved by using a metal binder together with WC that provides the plasticity of the composite material and, at the same time, has sufficiently high strength, melting point and impact elasticity.

The choice of a metal for the binder is restricted by the following conditions: this should withstand carburisation and in its molten state should adequately wet the carbide to be modified. Moreover, it is necessary that the carbide and the binding metal be soluble in each other. This provides their strong adhesion. For the case of WC, it is cobalt that best satisfies the mentioned requirements; that is why the first hard alloys that have found wide use in the industry were synthesised in the WC – Co system.¶

1. Hard alloys WC – Co

According to the phase diagram of the ternary W – Co – C system (see Fig. 12), at the low carbon content, the ternary compounds of the η-carbide type or the solid solution $Co_3W_3C_y$ based on η-carbides Co_4W_2C and Co_2W_4C can be formed. With further decrease in the carbon content, in the $Co_3W_3C_y$ solid solution, the triple phase diagram shows the appearance of a carbide with the approximate composition of $Co_6W_6C_y$. The mentioned ternary compounds and solid solutions exhibit enhanced brittleness; hence, in the synthesis of hard alloys, those compositions are used that lie in the WC – Co cross-section region where no ternary compounds can be formed. In commercial WC – Co alloys, the cobalt content varies from 4 to 18 mass % depending on their application.

The most important traditional operation in the technology of hard alloys is sintering of an item pressed from a powder mixture with an addition of a plasticiser[83,84] at 1600 – 1800 K. During the sintering of a WC – Co alloy, a certain amount of liquid phase, namely, molten cobalt, is formed. The wetting angle of WC with cobalt is zero, *i.e.*, molten cobalt completely wets the tungsten carbide grains and partly dissolves them; they crystallise upon subsequent cooling. In the sintering of a hard alloy, the following temperature intervals are considered:

— at 470 – 670 K, the plasticiser is removed;

— at 670 – 970 K, the admixtures of tungsten and cobalt oxides are reduced;

— at 1050 – 1400 K, individual carbide grains are welded together in their contact points;

— at 1400 – 1570 K, a solid solution of tungsten carbide in cobalt is formed, the sample shrinks and all cobalt passes to the luquid phase;

— at 1550 – 1670 K, due to the migration of carbide grains in the liquid phase, the sample acquires its final compact shape;

— the temperature increase up to 1770 – 1800 K is accompanied by additional dissolution of the WC grains in cobalt, on the one hand, and the growth of carbide grains due to the recrystallisation *via* the liquid phase, on the other hand; simultaneously, complete degassing of the alloy occurs;

— during cooling after the exposure at the maximum sintering temperature, the dissolved tungsten carbide deposits from the liquid phase onto the surface of carbide grains, which results in their growth.

In the ideal case, the sintered WC – Co alloy is two-phase, containing only WC grains and the metal binder between them. At a deficit or an excess of carbon, the alloy becomes three-phase and contains additionally either an η-phase of $Co_3W_3C_y$ (at carbon deficit) or graphite inclusions (at carbon excess). The graphite inclusions as well as the presence of very coarse (several times larger than the average size) WC grains substantially reduce the alloy service life.[85]

The average size of carbide phase grains increases noticeably upon sintering as compared with the grains in the original WC powder. Fine-grain alloys exhibit better performance and the use of fine-grain mixtures for the sintering allows higher quality alloys to be obtained. All other conditions being equal, the grain size in an alloy decreases with the decrease in the cobalt content due to the decrease in the liquid phase content and the deceleration of the grain growth by recrystallisation *via* the liquid phase; the grain size also decreases at a low content of carbon, which, however, results in the appearance of the brittle η-phase. Deceleration of the growth of carbide-phase grains in WC – Co alloys is achieved by their doping with other carbides. The most efficient dopant in this respect is vanadium carbide. Upon introduction of only 0.3 mass % of vanadium carbide, the average grain size of the carbide phase in fine-grain alloys is ~ 1 μm. To obtain fine-grain alloys, it is standard practice to include the long-term (up to 48 h) grinding of WC and Co powders in ethanol at the stage of mixture preparation.[86]

Over the past 20 years, the methods of synthesis of various substances and materials in the nanocrystalline state have been actively developed. In this state, the size of particles (grains, crystallites) does not exceed 40 nm.[87–90] Substances with particles measuring 40 – 100 nm are called submicrocrystalline.[89–91] Monographs[87–90] describe different methods of the synthesis of nanocrystalline powders and compact nanomaterials, the peculiarities of their microstructures, the methods of certification of nanomaterials, the effect of the particle (grain) size on the physical properties of substances. The manifestations of nanoscale effects in the structure and properties of metals, compounds and materials were reviewed.[92,93]

2. Nanostructured hard alloys

The most promising way to increase the production of nanostructured alloys with the reduced sintering temperature and the enhanced (due to the superfine-grain structure) hardness, strength, fracture toughness (crack-resistance) is to use nano- and submicrocrystalline carbides as the components of these alloys.[94,95] The decrease in the WC particle size even in the micron scale is accompanied by a noticeable increase in the wear resistance of WC – Co alloys, as well as the increase in their hardness and the compression and bending strength (Table 3, Fig. 18).[97,98]

¶ For the brief analysis of the data published from 1918 to 1923 on the development of hard alloys based on tungsten carbide in which such metals as Fe, Ni and Co were used as the binder, see a review.[15] The author of this review, K Schrüter, in 1925 patented the alloys WC – M (M = Co, Ni, Fe) in the USA with the priority from 1923. Later, similar alloys were developed in Sweden, Austria and other countries. In Russia, hard alloys based on tungsten carbide were manufactured under a trademark 'pobedit'.

Table 3. The effect of the WC grain size on certain properties of hard alloys WC – Co.[96]

Alloy composition (mass %)	Grain size /μm	Rockwell hardness /HRA	Density /g cm^{-3}	Bending strength /MPa	Compression strength /MPa	Modulus of elasticity /GPa	Relative wear resistance (%)
97WC – 3Co	1 – 2	92.5 – 93.2	15.3	1590	5860	641	100
94WC – 6Co	0.5 – 1.0	92.5 – 93.1	15.0	1790	5930	614	100
94WC – 6Co	1 – 2	91.7 – 92.2	15.0	2000	5450	648	58
94WC – 6Co	2 – 5	90.5 – 91.5	15.0	2210	5170	641	25
90WC – 10Co	0.5 – 1.0	90.7 – 91.3	14.6	3100	5170	620	22
90WC – 10Co	2 – 5	87.4 – 88.2	14.5	2760	4000	552	7

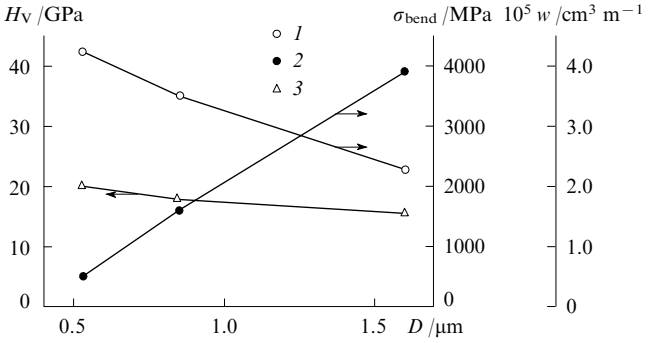


Figure 18. (*1*) Bending strength σ_{bend}, (*2*) wear rate (wear resistance) w and (*3*) hardness H_V as a function of the grain size D of the carbide phase of hard alloys WC – 6 mass % Co.[98]

The only exclusion known is the decrease in the bending strength of WC – 6 mass % Co alloys with the decrease in the grain size (see Table 3). The results of other studies demonstrate that the mechanical properties always improve with the transition from coarse-grain to fine-grain WC – Co alloys. For example, upon sintering of WC – 15 mass % Co nanopowders with the average particle size of 970, 490 and 30 nm at 1690 K the resulting alloys with the average grain size of 1350, 950 and 620 nm exhibited hardness of 13.8, 14.7 and 17.0 Gpa, respectively.[94] A hard alloy WC – 10 mass % of Co with the carbide phase of superfine structure (the WC grain size is smaller than 0.5 μm) exhibits microhardness of 19.3 GPa and a bending strength of 3890 MPa, whereas the same characteristics of a similar alloy with the grain size of 0.5 – 1.0 μm are 17.8 GPa and 3780 MPa.[99] Hard alloys WC – 6 mass % Co manufactured by 'Krupp Widia GmbH', which contain carbide-phase grains measuring 1.4 – 1.8, 0.8 – 0.9 and 0.5 – 0.6 μm, exhibit the bending strength of 2000, 3000 and 3800 MPa, the hardness of 15.8, 18.0 and 20.4 GPa, the abrasive wear resistance of 1.26%, 2.08% and 2.78%, respectively. A similar improvement in the mechanical properties with the decrease in the carbide-phase grain size was observed for hard alloys with larger (up to 15 mass %) cobalt content. The strength characteristics of conventional (with micron-scale grains) hard alloys based on WC are discussed in a monograph.[85]

Plasmochemical synthesis is among the most widely used chemical methods for obtaining fine-grain powders of nitrides and carbides.[100, 101] The main conditions for the production of fine-grain powders by this method are as follows: the reaction should proceed far from its equilibrium and the new-phase nucleation rate should be high as compared with the nuclei growth rate. Under real conditions of the plasmochemical synthesis, nanoparticles are produced upon fast cooling of the plasma flow in which the gas phase is condensed; this reduces the sizes of the particles formed and suppresses their coalescence upon collisions. The plasmochemical synthesis of carbides makes use of the low-temperature (3000 – 8000 K) hydrocarbon and argon plasma of the arc, glow, high-frequency and microwave discharges; elements and their halides and other compounds are used as the starting substances.[87] The characteristics of the powders synthesised depend on the starting materials, the process of synthesis and the reactor type. The particles obtained in plasmochemical reactions represent single crystals, have regular shapes and the sizes from 10 to 100 – 200 nm (and higher).

The plasmochemical synthesis is characterised by high rates of formation and condensation of substances, its efficiency is sufficiently high. The major disadvantages of this method are as follows: the wide size distribution of particles and, as a consequence, the presence of sufficiently coarse (up to 1 – 5 μm) particles, which means that the selectivity of the process is low, as well as high content of impurities in the resulting powder. To date, fine-grain powders of titanium, niobium, tantalum and tungsten carbides have been synthesised by the plasmochemical method.[87, 101 – 104] For instance, the synthesis of a submicrocrystalline WC powder with a specific surface area of 15 m^2 g^{-1} and a particle size not exceeding 300 nm,† which was conducted in an argon – hydrogen plasma from methane and tungsten hexafluoride, was reported.[104]

Synthesis of fine-grain tungsten carbide powders with the use of an arc plasmatron is described.[105] The plasmochemical synthesis produced a substance of the W – C – O system with a definite carbon-to-oxygen ratio, while the synthesis of the single-phase carbide as such was carried out in a tube furnace by the reduction of this product with hydrogen and CO. The specific surface area of synthesised WC varied from 5 – 6 to 50 m^2 g^{-1}. To produce the WC – Co furnace mixture, a cobalt powder with a specific surface area of 8 – 10 m^2 g^{-1}, which was synthesised by plasmochemical reduction of the oxide, was used. Sintering of the furnace mixture involved its hot pressing at 1370 – 1670 K and 10 – 50 MPa. The WC grain size in the samples sintered in the solid phase was ~100 nm.

A design of an electro-arc plasmatron for the plasmochemical synthesis (hydrogen plasma with the temperature of 3000 – 4000 K) of nanorystalline powders of refractory compounds including tungsten carbide with the particle sizes from 10 to 100 nm was reported.[106]

Low-temperature gas-phase synthesis of WC nanopowders is described.[107, 108] A two-step process was originally proposed [107] which included reduction of tungsten (its nanopowder) from tungstic acid salts, *i.e.*, the reductive decomposition of the precursor, followed by carburisation of tungsten in a CO-containing gas mixture. The synthesis produced a WC powder with the average grain size of 8 nm when conducted at 900 – 950 K and metastable lower carbide W_2C with particle measuring 13 – 19 nm when conducted at 600 – 800 K. A more straightforward one-step synthesis of the nanocrystalline WC carbide powder was described:[108] an H_2/CO gas mixture (2 : 1 or 1 : 1 molar ratios) was passed through ammonium tungstate or tungsten oxide powder at 800 – 1000 K; this directly led to the formation of nanocrystalline WC with particles < 10 nm. One important

† Note that WC has a density ρ = 15.6 g cm^{-3}; hence, the average particle size (diameter) in a powder of the total specific surface area S_{sp} = 15 m^2 g^{-1} should be $D = 6/\rho S_{sp} \approx 30$ nm, *i.e.*, 10 times smaller than reported.[104]

parameter of the single-step synthesis is the heating rate, which should provide the kinetic balance between the reduction and carburisation reactions. The heating rate of 2 deg min^{-1} is close to the optimum; moreover, heating even up to 1000 K resulted merely in a minor coarsening of WC particles as compared with heating to 800 K.

Mechanochemical synthesis in an cam-type mill produced hexagonal W_2C with the average particle size of 10 nm from a powder mixture of tungsten with the average particle size of up to 10 μm and carbon.[77]

To preserve the positive effect achieved due to the use of nanocrystalline powders for the production of hard alloys, the WC particles should retain small sizes during their sintering. In our studies,[109–111] we used the X-ray diffraction and magnetic susceptibility measurements to follow the changes in the thermal stability of a WC nanopowder that was obtained by the plasmochemical synthesis from WO_3 and propane at ~3300 – 3800 K in hydrogen plasma with the additional annealing in argon atmosphere at 1100 – 1300 K. The average particle size in the nanopowder was 50 – 55 nm. According to our studies, the particles in this powder retained the stable size when annealed in the temperature range from 300 to 1200 K, while the relaxation of microstresses in them began at ~600 K and ended at ~900 K.

The fine-grain structure of hard WC – Co alloys synthesised from WC powders is determined not only by the small size of the furnace mixture particles, but also by the way their sintering proceeds. Upon formation of the liquid phase, first, the smallest particles and, then, medium size particles pass to the melt, while coarser particles survive. Insofar as most nanoparticles are of the medium size, the number of crystallisation centres in the alloy will be sufficiently high. In the recrystallisation, tungsten carbide deposits on the surface of non-dissolved WC particles. Due to the excessive surface energy of small particles, they acquire a thicker layer of deposited tungsten carbide as compared with coarse particles. As a result, the size of carbide-phase particles levels off. In an ordinary hard alloy, the number of crystallisation centres is substantially smaller than in an alloy synthesised from the WC nanopowder; hence, a nanocrystalline alloy would have a more fine-grain and uniform structure as compared with an ordinary alloy. However, it should be borne in mind that the growth of grains in nanocrystalline compositions WC – Co can occur at ~1070 K,[112] *i.e.*, below the eutectic temperature of the W – Co – C system, which is equal to ~1600 K (nanopowders of WC – 15 mass % Co with the average particle size of 30 nm were studied;[112] the liquid phase appeared at ~1420 K during sintering). This means that, during the liquid-phase sintering of WC – Co nanopowders, the initial growth of carbide-phase grains occurs in the range of solid-phase sintering temperatures, whereas the subsequent liquid-phase sintering only leads to the coarsening of WC grains.[113]

Also note that the most compact (non-porous) alloys can be obtained provided the furnace mixture is not monodisperse, because obviously the total volume of a sample cannot be filled without voids with unisized particles. More compact packing is achieved due to the presence of different-sized particles in the furnace mixture, where the finer particles occupy the voids between the coarser particles. Analysis of the three-dimensional packing of spherical particles has shown[114] that a very high degree of the free space filling (~0.9) can be reached for their bimodal size distribution where, along with medium-size particles (D) that have the maximum share, the fraction of particles with a diameter ~0.1D is fairly high. In other words, the size-distribution curve of the particles should possess two maxima, the first of which (abundance) corresponds to the particles with the medium size D, while the second corresponds to the particles with the size ~0.1D.

Analysis of the literature data has shown that nanocrystalline or submicrocrystalline tungsten carbide can be synthesised by different methods. However, for the production of nanostructured hard alloys WC – Co, it is better that not only tungsten carbide, but the whole composition mixture WC – Co be in the nanocrystalline state. Such a mixture can be obtained by thermolysis of various precursors.[75] Particularly, heating can induce the following decomposition reactions resulting in the formation of WC and metallic cobalt:

$$(NH_4)_8[H_2Co_2W_{11}O_{40}]R \longrightarrow WC + Co,$$

$$[CoEn]_3WO_4 \longrightarrow WC + Co,$$

where R and En are alkyl and ethylenediamine, respectively.

Modern technologies of the production of nanocomposite mixtures WC – Co include several consecutive operations, namely, deposition from colloid solutions, cryogenic sputtering and drying, carbothemal reduction. Thus an efficient method for the production of nanocrystalline compositions of tungsten carbide and cobalt for manufacturing hard alloys is based on the co-deposition of WC and Co precursors from colloid solutions.[115,116] According to this method, colloid solutions of tungsten and cobalt salts {*e.g.*, $(NH_4)_6[H_2W_{12}O_{40}]\cdot 4H_2O$, $CoCl_2$, $Co(NO_3)_2$, $Co(CH_3COO)_2$} are dried by sputtering, then the obtained powder is subjected to the low-temperature carbothermal reduction in the fluidised bed and thus retains its high-dispersion state. This technology was patented[117] as the 'Spray Conversion Process (SCP)'. Insofar as the synthesis starts in the solution, the components (W and Co) are mixed on the molecular level, which favours the formations of an amorphous carburised powder.

The grain growth can be inhibited and the WC solubility in cobalt can be suppressed by adding up to 1 mass % of non-stoichiometric vanadium carbide to the mixture. The alloy obtained from this nanocrystalline composition demonstrates the optimum combination of high hardness and high strength; for example, its Vickers hardness reached 21.5 GPa, whereas the maximum hardness of an alloy with the same composition, which was obtained from a conventional WC powder, did not exceed 19.5 GPa.[115–118] The increase in the hardness and the decrease in WC grain size correlate with the increase in the vanadium carbide content in the alloy. Figure 19 illustrates the size distribution of grains in a sample of the WC – 6 mass % Co alloy obtained from a nanocomposite mixture prepared by the deposition method described above and containing 0.83 mass % of vanadium carbide, and in a sintered sample of a conventional alloy WC – 6 mass % Co containing 0.32 mass % of VC. As is seen, the average size of WC grains in the alloy synthesised from the

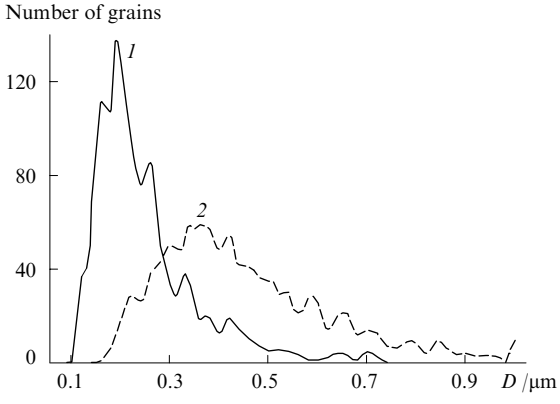


Figure 19. Size distribution of grains in WC – 6 mass % Co alloy samples.[119]
(*1*) Alloy sintered from a nanocomposite mixture of WC, Co and 0.83 mass % of VC, which was obtained by the co-deposition from colloid solution followed by drying and carbothermal reduction; the sample contained 1000 grains; (*2*) conventional fine-grain alloys WC – 6 mass % Co with 0.32 mass % of VC; the studied sample contained 948 grains.

amorphous nanocomposite powder is 250 nm, whereas an ordinary alloy has the grains almost twice larger (450 nm).

It was shown [119, 120] that each nanocomposite WC–Co particle with a size of ~75 μm consists of several millions of nanocrystalline WC grains measuring < 50 nm, which are distributed throughout the cobalt matrix (Fig. 20). Sintering of a nanocomposite tungsten carbide mixture with 6.8 mass % of Co and 1 mass % of vanadium carbide produced the alloys which contained 60% of the WC grains measuring < 250 nm and 20% measuring < 170 nm. A structure with still finer grains was obtained for an alloy which, in addition to tungsten carbide, contained 9.4 mass % of Co, 0.8 mass % of Cr_3C_2 and 0.4 mass % of VC_y. Upon its sintering at 1670 K, 60% of the tungsten carbide grains were < 140 nm and 20% were < 80 nm. A comparison of the nanoalloy with ordinary polycrystalline alloys of equal hardness have shown,[120] that the crack resistance of the nanoalloy is higher by a factor of 1.2–1.4 as compared with ordinary coarse-grain alloy.

The described nanocrystalline WC–Co composite powder with the carbide grain size of 20–40 nm is manufactured on the commercial scale in the USA as NANOCARB™. For the deposition of protective coatings by the thermal sputtering method, the nanocomposite multimodal (containing several fractions of carbide grains, *viz*., from 8 to 50 nm) WC–Co powder NANOMYTE™ was used.

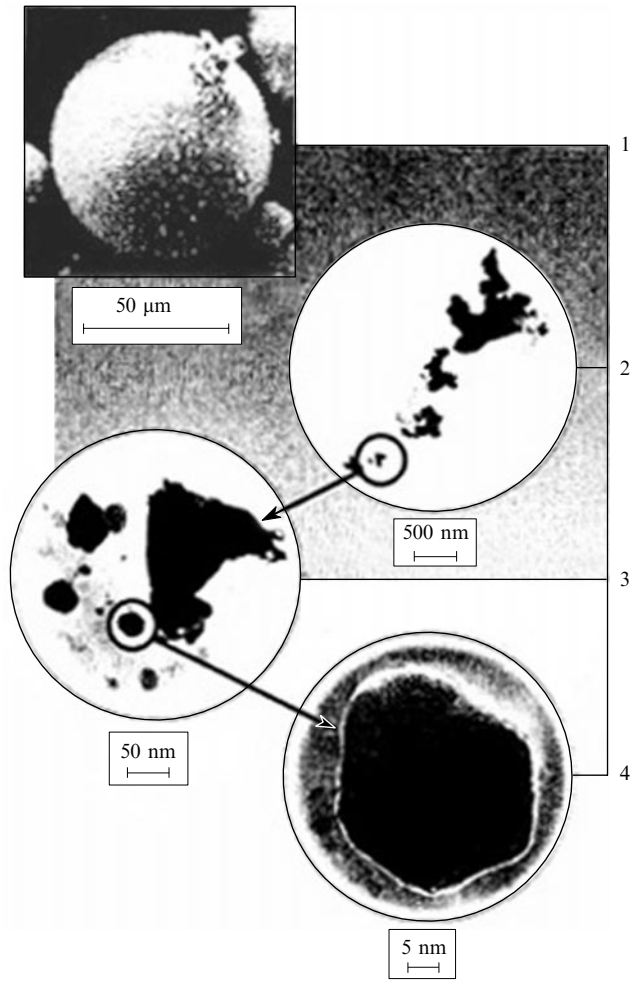


Figure 20. Distribution of WC grains in coarse particles of the amorphous nanocomposite mixture WC–6 mass % Co with 0.83 mass % of VC, which was obtained by the deposition from a colloid solution followed by drying and carbothermal reduction.[119, 120]
(*1*) A particle of a composite powder WC–Co measuring 75 μm, (*2*) particle fragments after grinding of the powder, (*3*) a polycrystalline cluster formed by WC grains in a cobalt matrix, (*4*) a WC grain measuring 30 nm.

Synthesis of a one-phase nanocrystalline WC powder by grinding tungsten and carbon in a ball mill at room temperature for 2.95×10^5 s is described;[121] the increase in the grinding time to 4.32×10^5 s afforded a nanopowder with the average grain size < 5 nm. Then different amounts of cobalt were added to the WC nanopowder, and grinding was continued for 2.6×10^5 s. The resulting nanocomposite mixtures WC–Co contained different amounts of cobalt, and the particles with the average size < 5 nm represented WC covered with a cobalt layer. Its pressing and hot sintering produced an alloy, which contained the carbide phase grains with the average size of ~100 nm. The hardness and the elasticity modulus of the alloys, which contained from 5 mass % to 12 mass % of Co varied in the ranges of 20–12 and 740–580 GPa, respectively.

It was already mentioned that the initial and the most active growth of carbide phase grains occurs in the sintering of WC–Co nanopowders in the temperature range of solid-state sintering. To decelerate the growth of grains in this region, it was proposed [122] to synthesise the nanostructured hard alloys WC–Co in an electric arc discharge. In this case, the stage of compacting of the nanopowder mixture is combined with its fast sintering and subsequent cooling of the sintered sample. The heating and cooling rates in this method are sufficiently high to avoid the sintering in the solid state and prevent the grain growth during the cooling. Thus a hard alloy was obtained [122] from a nanopowder of tungsten carbide containing 10 mass % of Co prepared by the SCP technology (see Refs 115–117) and had, on average, 50-nm coherent-scattering regions (according to X-ray diffraction data) or the average particle size of 200 nm (according to the data from scanning electron microscopy). The compacting pressure reached 300 MPa. When a current pulse was passed for several microseconds through a sample with the mass of 2.5 g, the energy (3 kJ g^{-1}) was liberated, which led to sintering. As a result, a hard alloy was obtained that had a density equal to 95% of its theoretical value and contained only WC and a fcc solid solution of tungsten carbide in cobalt. The average grain size in the carbide phase of this alloy was 120 nm according to data from electron microscopy; the measured modulus of elasticity was 550 GPa.[122]

A hard alloy WC–Co synthesised from a tungsten carbide powder with 30–50-nm particles [123] had a more uniform fine-grain structure and exhibited higher hardness and strength as compared with common hard alloys of the same composition. It was mentioned that the introduction of 3 mass %–5 mass % of tungsten carbide nanopowder to the standard furnace mixture containing coarse (1–4 μm) WC grains levels off the deviations in the hardness and strength of the resulting WC–Co alloy, *i.e*., stabilises the hard-alloy properties.

A virtually ideal version of mechanochemial synthesis, which is coupled with the synthesis of a nanocomposite mixture, was described.[124] A mixture of coarse (~75 μm) tungsten, graphite and cobalt powders was ground in an argon-filled ball mill for 100 h; the resulting nanocomposite WC–Co mixture contained cobalt and tungsten-carbide grains with the average diameter of 11–12 nm. In the hard alloy, which was obtained by cold pressing of the mixture followed by its sintering at 1310 K, most WC grain had a size < 200 nm, *i.e*., were several times smaller as compared with conventional alloys of the same composition. The sintered hard-alloy samples demonstrated the hardness of ~18 GPa and the relative density equal to 80% of the theoretical value. The possibility of sintering of a nanocomposite WC–Co powder mixture at lower temperatures as compared with coarse-grain mixtures is determined by the lower melting point of nanocrystalline cobalt as compared with coarse-grain cobalt.

Bearing in mind that even a small amount of non-stoichiometric vanadium carbide inhibits the growth of the carbide phase grains during the sintering, it was proposed [125] to synthesise V_8C_7 + WC powder mixtures in the first stage of the synthesis of WC–VC–Co alloys. Joint grinding of WC and V_8C_7 powders

with an addition of 0.5 mass % of Co for 48 h followed by their 3-h exposure at 1470 K to form their mixed (V,W)C carbide produced a mixture with the average particle size of 1.4 μm. Joint grinding of vanadium oxide, tungsten carbide and carbon was also carried out, which was followed by the carburisation of the resulting mixture at ~1470 K in the H_2/Ar atmosphere. In this case, the obtained powder had the particles with the average size of 1.8 μm.

The synthetic methods, the structure and mechanical properties of fine-grain hard alloys based on tungsten carbides were discussed briefly in a review.[126] Studies devoted to the microstructure, hardness and fracture toughness of hard WC–Co alloys [127] have shown that the hardness increases with a decrease in the thickness of the metal binder layer. It was also noted that the hardness measurements carried out at low loads or using a nanoindenter overestimate its value by ~2 GPa. The effects of the microstructure and the grain size of alloys WC–6 mass % of Co on their hardness in the temperature range from 80 to 1170 K was studied.[128] The examined alloys had the mictostructure typical of ordinary hard WC–Co alloys (Fig. 21). Figure 22 illustrates the changes in the hardness H_V of alloys with the average grain size of 0.6, 1.4 and 3.6 μm as a function of the temperature. It is evident that the alloys with a fine-grain structure are harder throughout this temperature range.

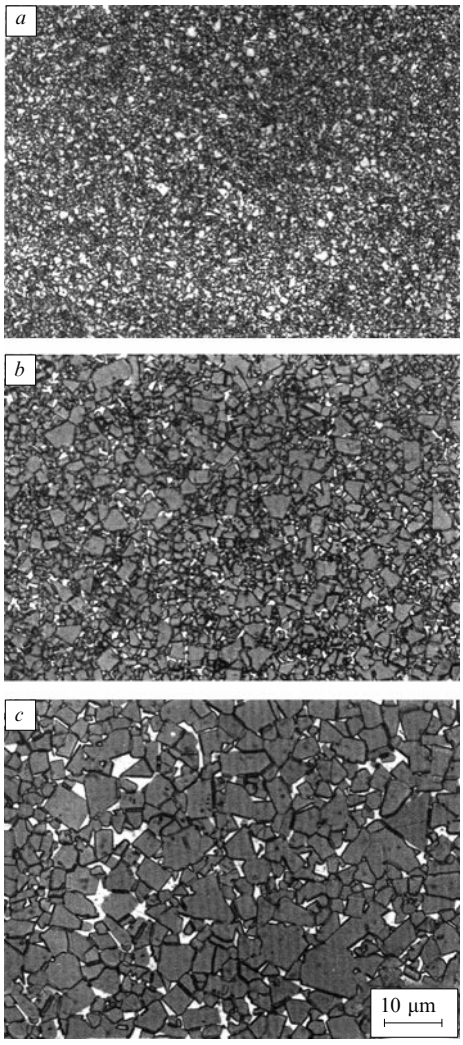


Figure 21. A typical microstructure of hard alloys WC–6 mass % Co with the average size of carbide phase grains of 0.6 (*a*), 1.4 (*b*) and 3.6 μm (*c*).[128]

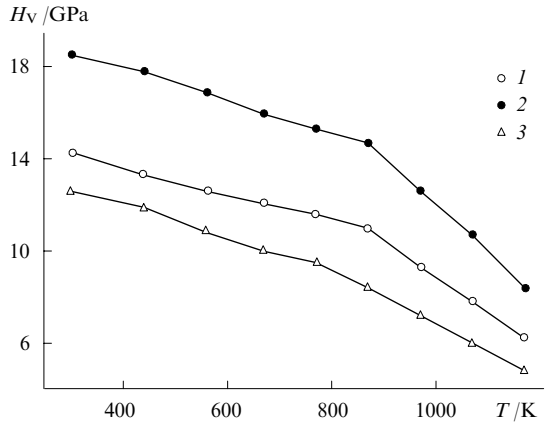


Figure 22. The effect of temperature of the Vickers hardness of WC–6 mass % Co alloys with the average size of carbide phase grains of 1.4 (*1*), 0.6 (*2*) and 3.6 μm (*3*).[128]
The measurements were performed under a load of 6 kg.

Recently, nanopowders of the WC–Co system came into use for synthesising nanocomposites that contain a diamond phase.[129, 130] A nanopowder WC–15 mass % of Co with tungsten carbide grains measuring 100 nm on average was pressed into samples of 8-mm diameter under a pressure of 100 and 300 MPa.[129] The samples were first heated to 1170 K in a hydrogen atmosphere to remove the oxide film and then sintered in vacuum at 1270–1470 K with 30-min exposure at the maximum sintering temperature. By varying the sintering time at the lowest temperature used, one could control the size and the arrangement of pores in the sample. Then, the samples were kept for 3 h at 1170 K in a flow of $H_2 + CH_4$ gas mixture to infiltrate the gas into the pores, after which they were simultaneously subjected to impact of high temperatures and pressures in order to reduce methane to carbon and transform carbon (graphite) into the diamond phase. The resulting superhard nanocomposite material contained ~45 vol.% of the diamond phase.[129] The diamond phase content in the synthesised nanocomposite seems to be significantly overrated.

A somewhat different method for the synthesis of WC–Co–diamond nanocomposites was proposed.[130] The initial mixture represented a powder mixture of WC with 15 mass % of Co; the average size of WC particles was 100 nm. The samples compacted under a pressure of 200 MPa were heated to 870 K in a hydrogen atmosphere to remove the oxide film and then sintered in vacuum at 1370 K for 30 min. The resulting porous samples with the 70% relative density were subjected to electrochemical etching in an aqueous $NaC_4H_5O_6$ solution. After the etching, the samples were washed with water, dried and then saturated with a gas mixture $H_2 + CH_4$, which contained 15% of methane. The infiltration of the gas into pores was carried out at 1170 K for 4 h. Then hydrostatic pressure of 8 GPa was applied at 1770 K to decompose methane in a catalytic reaction

$$CH_4 \longrightarrow C + 2H_2,$$

deposit carbon on the pore walls and transform it from the graphite state into the diamond state and also to condense the samples. The hardness of samples near their edges reached 32 ± 3 GPa, which was five times higher than in the bulk.

Thus, nowadays, there are different methods for the synthesis of nano- or submicrocrystalline tungsten carbides, WC–Co composite nanopowders and nanostructured hard WC–Co alloys. The available data suggest (see Table 3, Fig. 18) that the decrease in the size of carbide grains in hard WC–Co alloys is accompanied by noticeable increase in the abrasive wear resistance (by a factor of 2–3). Indeed, when drilling the printed circuit boards, the drills made of ultradispersed hard alloys prove to be

2–3 times more stable as compared with those made of standard alloys.[126] Therefore, it is reasonable to use the hard alloys with untradispersed and nanocrystalline structures, which combine the enhanced wear resistance, strength and fracture toughness, in those operations that require high wear resistance. However, it deserves mentioning that for ordinary alloys the same and even greater effect of the increase in the wear resistance can be achieved by the deposition of a wear-resistant coating.[131] This should be taken into account when assessing the economic profits associated with the use of nanostructured hard alloys.

VI. Conclusion

Hexagonal tungsten carbide is the most extensively used among all carbides of Group IV–VI transition metals. Originally, in the W–C system, only two hexagonal carbides W_2C_y (β-W_2C) and WC (δ-WC) were known, which despite their similar symmetry differ significantly, namely, lower carbide W_2C_y has a noticeable homogeneity region $WC_{0.34}$–$WC_{0.50}$, while hexagonal monocarbide δ-WC can have only the stoichiometric composition and contains no vacancies in the carbon sublattice. The non-stoichiometry of a disordered lower carbide W_2C_y, which is at equilibrium from 2700 K up to the melting point, is a prerequisite for its ordering with respect to both atoms and vacancies at lower temperatures. According to the neutron diffraction analysis, with decrease in the temperature, the following disorder–order transformation takes place in β-W_2C carbide:

$$\beta\text{-}W_2C \rightleftharpoons \varepsilon\text{-}W_2C.$$

The earlier concepts on the two consecutive transformations, *viz*., the disorder–order transformation to form the orthorhombic β′-W_2C phase of the PbO_2 type

$$\beta\text{-}W_2C \rightleftharpoons \beta'\text{-}W_2C$$

and the order–disorder transformation to form the trigonal β″-W_2C phase of the *C*6 type

$$\beta'\text{-}W_2C \rightleftharpoons \beta''\text{-}W_2C$$

were not confirmed by the neutron diffraction analysis of the W_2C structure.

One peculiarity of lower tungsten carbide is that at 1523 K it undergoes the eutectoid decomposition to give tungsten and δ-WC and thus does not exist at lower temperatures. In the 1960s, an additional compound highly non-stoichiometric with respect to carbon, namely, cubic carbide γ-WC_{1-x} was discovered in the W–C system. The region of the existence of equilibrium of this carbide is very wide with respect to composition (from $WC_{0.58-0.59}$ to $WC_{1.00}$) and very narrow with respect to temperature (from ~3060 to ~2990–3020 K); however, due to quenching from high temperature, it can be preserved in the metastable state at 300 K. The temperature of the equilibrium transformation

$$\gamma\text{-}WC_{1-x} \rightleftharpoons \delta\text{-}WC$$

is 3000–3010 K; however, the temperature of the non-equilibrium transformation of the quenched cubic carbide γ-WC_{1-x} to give hexagonal δ-WC, which occurs on heating, is still unknown.

Studies on the W–C system are also important from the practical viewpoint, because tungsten carbide is used in the production of hard alloys applied in the metal working and drilling. The traditional basis for such alloys is hexagonal stoichiometric carbide WC (δ-WC); to date, no attempts were undertaken to use cubic carbide γ-$WC_{1.0}$ of the stoichiometric composition or non-stoichiometric cubic carbide γ-WC_{1-x} for these purposes. The cubic structure of tungsten carbide can apparently be stabilised by the addition of other cubic carbides, for example, VC_y. The use of cubic tungsten carbide with VC_y additives as the basis for hard alloys can also provide the thermal stability of the carbide phase and the fine-grain structure of the alloy.

Yet another direction in the application of tungsten carbide, which was actively developed in the past 20 years, concerns the nanostructured hard alloys. In the systems W–C and W–C–Co, the nanostructured carbides or nanocomposites of the WC–Co and WC–Co–diamond types were obtained. Their synthesis became possible due to the use of new and, as a rule, combined synthetic methods and non-traditional procedures such as co-deposition of tungsten and cobalt from colloid solutions, thermal decomposition of precursors, plasmochemical reduction, mechanosynthesis, *etc*. The particle sizes in nanocomposites can be very low (10–40 nm); however, the problem of the conservation of the small particles during sintering of a hard alloy is not yet solved completely. Nonetheless, the microstructure of newly developed ultradispersed hard alloys contains carbide-phase grains with the average size of 100–250 nm, which provides the noticeable increase in their hardness, wear resistance and other performance characteristics. The introduction of small amounts of vanadium carbide favours the retention of small-sized grains in nanostructured hard alloys.

On the whole, the studies of tungsten carbides and the related phase equilibria in both the W–C system and more complex systems containing tungsten carbides contribute to the development of fundamental concepts on the nature of refractory compounds of transition metals and serve as the basis for their wide application in the future.

This review has been written with the financial support of the Russian Foundation for Basic Research (Project No. 06-03-32 047a).

References

1. A I Gusev, A A Rempel *Strukturnye Fazovye Perekhody v Nestekhiometricheskikh Soedineniyakh* (Structural Phase Transitions in Non-stoichiometric Compounds) (Moscow: Nauka, 1988)
2. A I Gusev *Fizicheskaya Khimiya Nestekhiometricheskikh Tugoplavkikh Soedinenii* (Physical Chemistry of Non-stoichiometric Refractory Compounds (Moscow: Nauka, 1991)
3. A I Gusev, A A Rempel *Nestekhiometriya, Besporyadok i Poryadok v Tverdom Tele* (Non-stoichiometry, Disorder and Order in Solid) (Ekaterinburg: Urals Branch of the Russian Academy of Science, 2001)
4. A I Gusev, A A Rempel, A J Magerl *Disorder and Order in Strongly Non-stoichiometric Compounds: Transition Metal Carbides, Nitrides and Oxides* (Berlin, Heidelberg, New York, London: Springer, 2001)
5. A L Ivanovskii, V P Zhukov, V A Gubanov *Elektronnoe Stroenie Tugoplavkikh Karbidov i Nitridov Perekhodnykh Metallov* (Electronic Structure of Refractory Carbides and Nitrides of Transition Metals) (Moscow: Nauka, 1990)
6. V N Lipatnikov, A I Gusev *Uporyadochenie v Karbidakh Titana i Vanadiya* (Ordering in Titanium and Vanadium Carbides) (Ekaterinburg: Urals Branch of the Russian Academy of Science, 2000)
7. H J Goldschmidt *Interstitial Alloys* (London: Butterworths, 1967)
8. R B Kotel'nikov, S N Bashlykov, Z G Galiakbarov, A I Kashtanov *Osobo Tugoplavkie Elementy i Soedineniya* (Extra Refractory Elements and Compounds) (Moscow: Metallurgiya, 1969)
9. E K Storms *The Refractory Carbides* (New York, London: Academic Press, 1967)
10. L E Toth *Transition Metal Carbides and Nitrides* (New York, London: Academic Press, 1971)
11. R A Andrievskii, A G Lanin, G A Rymashevskii *Prochnost' Tugoplavkikh Soedinenii* (Strength of Refractory Compounds) (Moscow: Metallurgiya, 1974)
12. H Holleck *Binäre und Ternäre Carbid- und Nitridsysteme der Übergangsmetalle* (Berlin, Stuttgart: Gebrüder Borntraeger, 1984)
13. H Moissan *Compt. Rend.* **116** 1225 (1893)

14. H Moissan *Compt. Rend.* **125** 839 (1897)
15. K Schrüter *Iron Age* **133** 27 (1934)
16. T B Massalski, J L Murray, L H Bennet, H Baker, L Kasprzak (Eds), in *Binary Alloy Phase Diagrams* Vol. 1 (Metals Park, OH: American Society for Metals, 1987) p. 599
17. T B Massalski, J L Murray, L H Bennet, H Baker, L Kasprzak (Eds), in *Binary Alloy Phase Diagrams* Vol. 1 (2nd Ed.) (Metals Park, OH: American Society for Metals, 1990) p. 895
18. E Rudy, S Windisch *J. Am. Ceram. Soc.* **50** 272 (1967)
19. E Rudy, S Windisch, J R Hoffman, in *Ternary Phase Equilibria in Transition Metal – Boron – Carbon – Silicon Systems (Tech. Doc. Report AFML-TR-65-2. Metals and Ceramics Division)* (Wright-Patterson Air Force Base Ohio, USA: Air Force Materials Laboratory, 1966) Pt. I, vol. VI, p. 1
20. E Rudy, in *Compendium of Phase Diagram Data. Ternary Phase Equilibria in Transition Metal – Boron – Carbon – Silicon Systems (Tech. Doc. Report AFML-TR-65-2. Metals and Ceramics Division)* (Wright-Patterson Air Force Base Ohio, USA: Air Force Materials Laboratory, 1966) Pt. V, p. 735
21. E Rudy, J R Hoffman *Planseeber. Pulvermet.* **15** 174 (1967)
22. R V Sara *J. Am. Ceram. Soc.* **48** 251 (1965)
23. A E McHale (Ed.), in *Phase Equilibria Diagrams. Phase Diagrams for Ceramists* Vol. X (Westerville, OH: American Ceramics Society, 1994) p. 272
24. N P Lyakishev (Ed.) *Diagrammy Sostoyaniya Dvoinykh Metallicheskikh Sistem* (State Diagrams of Binary Metal Systems) (Moscow: Mashinostroenie, 1996) Vol. 1, p. 778
25. K Yvon, H Nowotny, F Benesovsky *Monatsh. Chem.* **99** 726 (1968)
26. A Harsta, S Rundqvist, J O Thomas *Acta Chem. Scand. A* **32** 891 (1978)
27. A Lönnberg, T Lundström, R Tellgren *J. Less-Common Met.* **120** 239 (1986)
28. T Epicier, J Dubois, C Esnouf, G Fantozzi *Compt. Rend. Acad. Sci. Paris, Ser. II* **297** 215 (1983)
29. T Epicier, J Dubois, C Esnouf, G Fantozzi, P Convert *Acta Metall.* **36** 1903 (1988)
30. J J Lander, L H Germer *Transact. AIME* **175** 661 (1948)
31. G Lautz, D Schneider *Z. Naturforsch. A* **16** 1368 (1961)
32. H J Goldschmidt, J A Brand *J. Less-Common Met.* **5** 181 (1963)
33. E Parthe, V Sadagopan *Acta Crystallogr.* **16** 202 (1963)
34. L N Butorina, Z G Pinsker *Kristallografiya* **5** 585 (1960) [a]
35. H D Heetderks, E Rudy, T Eckert *Planseeber. Pulvermet.* **13** 104 (1965)
36. P Ronsheim, L E Toth, A Mazza, E Pfender, B Mitrofanov *J. Mater. Sci.* **16** 2665 (1981)
37. R H Willens, E Buehler *Appl. Phys. Lett.* **7** 25 (1965)
38. R H Willens, E Buehler, B T Matthias *Phys. Rev.* **159** 327 (1967)
39. E Krainer, J Robitsch *Planseeber. Pulvermet.* **15** 46 (1967)
40. S A Gromilov, S A Kinelovskii *Zh. Strukt. Khim.* **44** 486 (2003) [b]
41. US P. 3084534 (1963)
42. S V Vonsovskii, Yu A Izyumov, E Z Kurmaev *Sverkhprovodimost' Perekhodnykh Metallov, ikh Splavov i Soedinenii* (Superconductivity of Transition Metals, Their Alloys and Compounds) (Moscow: Nauka, 1977)
43. E Krainer, J Robitsch *Planseeber. Pulvermet.* **15** 179 (1967)
44. A S Kurlov, A I Gusev *Neorg. Mater.* **42** 156 (2006) [c]
45. L N Butorina *Kristallografiya* **5** 233 (1960) [a]
46. A Y Liu, R M Wentzcovitch, M L Cohen *Phys. Rev. B* **38** 9483 (1988)
47. A A Rempel, R Würschum, H-E Schaefer *Phys. Rev. B* **61** 5945 (2000)
48. A A Rempel, H-E Schaefer, M Forster, A I Girka, in *Materials Research Society Symposium Proceedings. Covalent Ceramics II: Non-oxides* (Eds A R Barron, G S Fischman, M A Fury, A F Hepp) (Pittsburgh, PA: Materials Research Society, 1994) Vol. 327, p. 301
49. M J Puska, M Šob, G Brauer, T Korhonen *J. Physique IV* **5** C1-135 (1995)
50. E Rudy, S Windisch, Y A Chang, in *Ternary Phase Equilibria in Transition Metal – Boron – Carbon – Silicon Systems (Tech. Doc. Report AFML-TR-65-2. Metals and Ceramics Division)* (Wright-Patterson Air Force Base Ohio, USA: Air Force Materials Laboratory, 1965) Pt. I, vol. I, p. 1
51. E Rudy, S Windisch, A J Stosick, J R Hoffman *Transact. AIME* **239** 1247 (1967)
52. P Rautala, J T Norton *Transact. AIME* **194** 1045 (1952)
53. J Gurland *Transact. AIME* **200** 285 (1954)
54. B B Pollock, H H Stadelmaier *Metall. Transact.* **1** 767 (1970)
55. P Ettmayer, R Suchentrunk *Monatsch. Chem* **101** 1098 (1970)
56. T Johansson, B Uhrenius *Metal. Sci.* **12** 83 (1978)
57. V Adelsköld, A Sundelin, A Westgren *Z. Anorg. Allgem. Chem.* **212** 401 (1933)
58. N Schönberg *Acta Metall.* **2** 837 (1954)
59. A Harsta, T Johansson, N Rundqvist, J O Thomas *Acta Chem. Scand. A* **31** 260 (1977)
60. A F Guillermet *Metall. Transact. AIME A* **20** 935 (1989)
61. L Kaufman, H Bernstein *Computer Calculation of Phase Diagrams* (New York: Academic Press, 1970)
62. A Sundman, I Ansara, M Hillert, G Inden, H-L Lukas, K C H Kumar *Z. Metallkunde* **92** 526 (2001)
63. P Villars, A Prince, H Okamoto, in *Handbook of Ternary Alloy Phase Diagrams* Vol. 5 (Metals Park, OH: American Society for Metals, 1995) p. 6585
64. E S Alekseev, P G Arkhipov, S V Popova *Phys. Status Solidi B* **110** K151 (1982)
65. L F Mattheiss, D R Hamann *Phys. Rev. B* **30** 1731 (1984)
66. V P Zhukov, V A Gubanov *Solid State Commun.* **56** 51 (1985)
67. V P Zhukov, V A Gubanov, T Jarlborg *J. Phys. Chem. Solids* **46** 1111 (1985)
68. V P Zhukov, V A Gubanov *Izv. Akad. Nauk SSSR, Neorg. Mater.* **22** 1665 (1986) [c]
69. A T Matthias, J K Hulm *Phys. Rev.* **87** 799 (1952)
70. N I Medvedeva, A L Ivanovskii *Fiz. Tv. Tela* **43** 452 (2001) [d]
71. A W Weimer (Ed.) *Carbide, Nitride and Boride Materials Synthesis and Processing* (London: Chapman and Hall, 1997)
72. Y G Gogotsi, R A Andrievski (Eds) *Materials Science of Carbides, Nitrides and Borides* (Dordrecht: Kluwer Academic, 1999)
73. BRD P. 198 07 589 A (1998)
74. V P Bondarenko, E G Pavlotskaya *Porosh. Metall.* (9 – 10) 21 (1995) [e]
75. N T Kuznetsov, in *Materials Science of Carbides, Nitrides and Borides* (Eds Y G Gogotsi, R A Andrievski) (Dordrecht: Kluwer Academic, 1999) p. 223
76. E G Avvakumov (Ed.) *Mekhanokhimicheskii Sintez v Neorganicheskoi Khimii* (Mechanochemical Synthesis in Inorganic Chemistry) (Novosibirsk: Nauka, 1991)
77. V Yu Davydkin, L I Trusov, P Yu Butyagin, V V Moskvin, I V Kolbanev, V I Novikov, S S Plotkin, in *Mekhanokhimicheskii Sintez v Neorganicheskoi Khimii* (Mechanochemical Synthesis in Inorganic Chemistry) (Ed. E G Avvakumov) (Novosibirsk: Nauka, 1991) p. 183
78. Yu V Baikalova, O I Lomovsky *J. Alloys Compd.* **297** 87 (2000)
79. J H Westbrook, E R Stover, in *High-temperature Materials and Technology* (Eds I E Campbell, E M Sherwood) (New York: Wiley, 1967) p. 312
80. M S Koval'chenko, V V Dzhemelinskii, V N Skuratovskii, Yu G Tkachenko, D Z Yurchenko, V I Alekseev *Porosh. Metall.* (8) 87 (1971) [e]
81. A G Atkins, D Tabor *Proc. R. Soc. London* **292** 441 (1966)
82. G V Samsonov, V K Vitryanyuk, F I Chaplygin *Karbidy Vol'frama* (Carbides of Tungsten) (Kiev: Naukova Dumka, 1974)
83. R Kiffer, F Benezovskii *Tverdye Splavy* (Hard Alloys) (Moscow: Metallurgiya, 1971)
84. N I Romanova, P G Chekulaev, V I Dusev, T A Livshits, M N Kurdov, in *Metallokeramicheskie Tverdye Splavy* (Powder Metallurgical Hard Alloys) (Moscow: Metallurgiya, 1970) p. 144
85. M G Loshak *Prochnost' i Dolgovechnost' Tverdykh Splavov* (Strength and Durability of Hard Alloys) (Kiev: Naukova Dumka, 1984)
86. T A Emel'yanova, N B Kobitskaya, T B Gorbacheva *Metally* (1) 75 (1992)
87. A I Gusev *Nanokristallicheskie Materialy: Metody Polucheniya i Svoistva* (Nanocrystalline Materials: Methods of Production and Properties) (Ekaterinburg: Urals Branch of the Russian Academy of Science, 1998)

88. A I Gusev, A A Rempel *Nanokristallicheskie Materialy* (Nanocrystalline Materials) (Moscow: Fizmatlit – Nauka, 2000)
89. A I Gusev, A A Rempel *Nanocrystalline Materials* (Cambridge: Cambridge Int. Sci. Publ., 2004)
90. A I Gusev *Nanomaterialy, Nanostruktury, Nanotekhnologii* (Nanomaterials, Nanostructures and Nanotechnologies) (Moscow: Fizmatlit – Nauka, 2005)
91. R Z Valiev, I V Aleksandrov *Nanostrukturnye Materialy, Poluchennye Intensivnoi Plasticheskoi Deformatsiei* (Nanostructural Materials, Production by Intense Plastic Deformation) (Moscow: Logos, 2000)
92. A I Gusev *Usp. Fiz. Nauk* **168** 55 (1998) [*Physics-Uspekhi* **41** 49 (1998)]
93. A I Gusev, in *Dekker Encyclopedia of Nanoscience and Nanotechnology* Vols 1 – 5 (Eds J A Schwarz, C Contescu, K Putyera) (New York: Am. Sci. Publ., 2004) p. 2289
94. S Berger, R Porat, R Rosen *Progr. Mater. Sci.* **42** 311 (1997)
95. A I Gusev, A S Kurlov *Metally Evrazii* (2) 42 (2005)
96. H J Scussel, in *Friction, Lubrication and Wear Technology. (Metals Handbook ASM)* Vol. 18 (10th Ed) (Metals Park, OH: American Society for Metals, 1992) p. 795
97. H W Daub, K Dreyer, A Happe, H Holzhauer, D Kassel, in *Pulvermetallurgie in Wissenschaft und Praxis* Bd. 11 (Ed. H Kolaska) (Oberursel: DGM Informationsgesellschaft Verlag, 1995) p. 285
98. R Vaâen, D Stöver *J. Mater. Proc. Technol.* **92 – 93** 77 (1999)
99. W D Schubert, A Bock, B Lux, in *Proceedings of the 13th International Plansee Seminar* Vol. 4 (Eds H Bildstein, R Eck) (Reutte: Metallwerk Plansee, 1993) p. 283
100. T N Miller *Izv. Akad. Nauk SSSR, Neorg. Mater.* **15** 557 (1979) [c]
101. T Ya Kosolapova, G N Makarenko, D P Zyatkevich *Zh. Vsesous. Khim. o-va im. D I Mendeleeva* **24** 228 (1979) [f]
102. B H Kear, P R Strutt *Nanostruct. Mater.* **6** 227 (1995)
103. I V Blinkov, A V Ivanov, I E Orekhov *Fiz. Khim. Obrabot. Mater.* (2) 73 (1992)
104. V I Shishkovskii, Yu D Kopytin, N E Gubaidullin, in *Ul'tradispersnye Poroshki, Materialy i Nanostruktury: Poluchenie, Svoistva, Primenenie. Materialy Mezhregional'noi Konferentsii* (Superdispersed Powders, Materials and Nanostructures: Productions, Properties and Applications. Materials of Interregional Conference) (Krasnoyarsk: Krasnoyarsk State Technical University, 1996) p. 56
105. Yu V Blagoveshchenskii, E A Danilkin, T P Egorikhina, V I Terekhov, in *Fizikokhimiya Ul'tradispersnykh Sistem. Materialy IV Vserossiiskoi Konferentsii* (Physical Chemistry of Superdispersed Systems. Proceedings of IVth All-Russian Conference) (Moscow: Moscow Engineering and Physics Institute, 1998) p. 274
106. A V Lebedev, Yu V Blagoveshchenskii, V A Moldaver, in *Fizikokhimiya Ul'tradispersnykh Sistem. Materialy V Vserossiiskoi Konferentsii* (Physical Chemistry of Superdispersed Systems. Proceedings of Vth All-Russian Conference) (Moscow: Moscow Engineering and Physics Institute, 2000) p. 145
107. L Gao, B H Kear *Nanostruct. Mater.* **5** 555 (1995)
108. L Gao, B H Kear *Nanostruct. Mater.* **9** 205 (1997)
109. A S Kurlov, S Z Nazarova, A A Rempel, in *Nanotekhnologiya i Fizika Funktsional'nykh Nanokristallicheskikh Materialov* (Nanotechnologies and Physics of Functional Nanocrystalline Materials) (Ed. V V Ustinov, N I Noskova) (Ekaterinburg: Institute of Physics of Metals, Urals Branch of the Russian Academy of Sciences, 2005) Vol. 1, p. 59
110. A S Kurlov, S Z Nazarova, A I Gusev *Dokl. Akad. Nauk* **405** 218 (2005) [g]
111. A S Kurlov, S Z Nazarova, A I Gusev *Pis'ma Zh. Eksp. Teor. Fis.* **82** 567 (2005) [h]
112. P Arató, L Bartha, R Porat, S Berger, A Rosen *Nanostruct. Mater.* **10** 245 (1998)
113. M Sommer, W-D Schubert, E Zobetz, E Warbichler *Int. J. Refract. Met. Hard Mater.* **20** 41 (2002)
114. S V Anishchik, N N Medvedev *Phys. Rev. Lett.* **75** 4314 (1995)
115. L E McCandlish, B H Kear, B K Kim *Nanostruct. Mater.* **1** 119 (1992)
116. L Wu, J Lin, B K Kim, B H Kear, L E McCandlish, in *Proceedings of the 13th International Plansee Seminar* Vol. 3 (Eds H Bildstein, R Eck) (Reutte: Metallwerk Plansee, 1993) p. 667
117. L E McCandlish, B H Kear, S J Bhatia, US P. 5352269 (1994)
118. Z Fang, J W Eason, in *Proceedings of the 13th International Plansee Seminar* Vol. 4 (Eds H Bildstein, R Eck) (Reutte: Metallwerk Plansee, 1993) p. 625
119. P Seegopaul, L E McCandlish *Adv. Powder Metall. Part. Mater.* **3** 13 (1995)
120. P Seegopaul, L E McCandlish, F M Shinneman *Int. J. Refract. Met. Hard Mater.* **15** 133 (1997)
121. M S El-Eskandarany, A A Mahday, H A Ahmed, A H Amer *J. Alloys Compd.* **312** 315 (2000)
122. X Y Wu, W Zhang, W Wang, F Yang, J Y Min, B Q Wang, J D Guo *J. Mater. Res.* **19** 2240 (2004)
123. N I Borisenko, V A Moldaver, A V Lebedev, N V Kobzarev, in *Fizikokhimiya Ul'tradispersnykh (Nano-) Sistem (Sbornik Nauchnykh Trudov VI Vserossiiskoi Konferentsii)* [Physical Chemistry of Superdispersed (Nano-) Systems (Proceedings of the VIth All-Russian Conference)] (Moscow: Moscow Engineering and Physics Institute, 2003) p. 505
124. M A Xueming, J I Gang *J. Alloys Compd.* **245** L30 (1996)
125. B Osborne, L Cornish *Int. J. Refract. Met. Hard Mater.* **15** 163 (1997)
126. L I Klyachko, V A Fal'kovskii, A M Khokhlov *Tverdye Splavy na Osnove Karbida Vol'frama s Tonkodispersnoi Strukturoi* (Hard Alloys Based on Tungsten Carbide with Fine Structure) (Moscow: Ruda i Metally, 1999)
127. K Jia, T E Fischer, B Gallois *Nanostruct. Mater.* **10** 875 (1998)
128. Yu V Milman, S Chugunova, V Goncharuck *Intern. J. Refract. Met. Hard Mater.* **15** 97 (1997)
129. R K Sadangi, O A Voronov, B H Kear *Nanostruct. Mater.* **12** 1031 (1999)
130. M Jain, R K Sadangi, W R Cannon, B H Kear *Scr. Mater.* **44** 2099 (2001)
131. V I Tret'yakov *Osnovy Metallovedeniya i Tekhnologii Proizvodstva Spechennykh Tverdykh Splavov* (Foundations of Metal Research and Technology of Production of Sintered Hard Alloys) (Moscow: Metallurgiya, 1976)

[a] — *Crystallogr. Rep. (Engl. Transl.)*
[b] — *J. Struct. Chem. (Engl. Transl.)*
[c] — *Inorg. Mater. (Engl. Transl.)*
[d] — *Phys. Solid. State (Engl. Transl.)*
[e] — *Power Metall. Met. Ceram. (Engl. Transl.)*
[f] — *Mendeleev Chem. J. (Engl. Transl.)*
[g] — *Dokl. Chem. (Engl. Transl.)*
[h] — *J. Theor. Exp. Phys. Lett. (Engl. Transl.)*